University of Alberta
Printing Department

THE UNIVERSITY OF ALBERTA

CRUSTAL STRUCTURE IN WESTERN CANADA

by

GERRIT T. F. R. MAUREAU

A THESIS
SUBMITTED TO THE FACULTY OF GRADUATE STUDIES
IN PARTIAL FULFILLMENT OF THE REQUIREMENTS FOR THE DEGREE
OF MASTER OF SCIENCE

DEPARTMENT OF PHYSICS
EDMONTON, ALBERTA

NOVEMBER, 1964

UNIVERSITY OF ALBERTA

FACULTY OF GRADUATE STUDIES

The undersigned certify that they have read, and recommend to the Faculty of Graduate Studies for acceptance, a thesis entitled CRUSTAL STRUCTURE IN WESTERN CANADA, submitted by Gerrit T. F. R. Maureau, in partial fulfillment of the requirements for the degree of Master of Science.

Abstract

In the summers of 1963 and 1964 a double-ended refraction profile was shot between Suffield, Alberta and Swift Current, Saskatchewan. A six layer earth model was obtained from these data, the crustal thickness under the east shot point (Swift Current) being 42 kms and the thickness under the west shot point (Suffield) being 51 kms. These data are similar in general form to those reported by Meyer and McCamy in Montana, just south of our line.

Previous control west from Suffield has been extended into the Rocky Mountains. Since these data are not reversed, definitive interpretation is not possible. Some alternative interpretations are presented.

Spectral analyses were also carried out on many of the records. Power spectra indicate that there is little change in frequency with distance from the shot point. They do, however, indicate that there are two dominant frequencies of seismic information, one at about 5 cps and another at about 10 cps. Shot environment determines which of these two is more important.

Abstract

In the summers of 1963 and 1964 a double-ended refraction profile was shot between Suffield, Alberta and Swift Current, Saskatchewan. A six layer earth model was obtained from these data, the crustal thickness under the east shot point (Swift Current) being 42 kms and the thickness under the west shot point (Suffield) being 51 kms. These data are similar in general form to those reported by Meyer and McCamy in Montana, just south of our line.

Previous control west from Suffield has been extended into the Rocky Mountains. Since these data are not reversed, definitive interpretation is not possible. Some alternative interpretations are presented.

Spectral analyses were also carried out on many of the records. Power spectra indicate that there is little change in frequency with distance from the shot point. They do, however, indicate that there are two dominant frequencies of seismic information, one at about 5 cps and another at about 10 cps. Shot environment determines which of these two is more important.

Acknowledgements

I wish to thank Dr. G. L. Cumming for having suggested this problem to me. Without his many ideas, help and guidance the completion of this thesis would not have been possible.

I also wish to thank Dr. E. R. Kanasewich for many helpful discussions which guided me in the course of my work.

Mr. M. D. Burke, our geophysics technician, was especially helpful in solving the many technical difficulties encountered in using the instruments. I am also grateful to Mr. Burke for his help in preparing the section on instrumentation.

Had it not been for the aid of the USGS Crustal Studies Group of Denver, Colorado, and Dr. Hugh White of the Dominion Astrophysical Observatory, Victoria, B. C., the westerly extension of our Suffield - Vulcan refraction line would not have been possible.

Technical assistance in all phases of the operation was provided by Messrs. Dave Robertson, Ken Roxborough, Bob Stuart, A. Kumar, Stanley Allen, Ross Lasby, Martin Murenbeeld, and Charles McCloughan. I am grateful for their help.

The power spectra were computed using a program prepared by Dr. R. M. Ellis.

British American Oil Co., Ltd. provided three continuous velocity logs which were very useful in computing the near surface structure at both shot points. Their aid is gratefully acknowledged.

The author was supported during the course of his research by a Graduate Teaching Assistantship from the Department of Physics, University of Alberta, and by a scholarship from the Society of Exploration Geophysicists Foundation.

This project was sponsored by the Advanced Research Projects Agency, Project Vela-Uniform, funds administered by the Air Force Cambridge Research Laboratories, Bedford, Massachusetts, and by the Defence Research Board of Canada. Technical assistance from the latter group was provided by the Suffield Experimental Station, Ralston, Alberta, and is gratefully acknowledged.

TABLE OF CONTENTS

Contents Page

Chapter 4

LIST OF FIGURES

Appendix Figures

LIST OF TABLES

The Long Range Refraction Survey

Ever since man has been inquisitive enough to study the nature of his surroundings, the structure of the earth has presented a major problem. His descriptive studies of the surface of the earth had revealed only superficial information about the structure of our planet. With the advent of the seismometer and the development of the science of seismology (a geophysical science which is concerned with the study of earthquakes and the measurement of the elastic properties of the earth), man has been able to gain a better insight into the structure of the interior of the earth. From these measurements of earthquakes the geophysicist was able to distinguish three broad regions in the earth. These were:

1. The crust of the earth. This region comprises the outer shell of the earth, and measures about 35 kms thick under continents and about 10 to 15 kms thick under oceans. The base of the crustal layer is defined by the Mohorovičić discontinuity. This is a seismic discontinuity, and is recognized throughout the world.
2. The mantle. This region of the earth extends down from the base of the crust to a depth of 2900 kms. This layer is believed to be composed of iron rich silicates, although near the Mohorovičić discontinuity it is believed to be an

ultra-basic silicate much like dunite, peridotite or eclogite. Since the mantle will sustain both longitudinal and shear waves it is thought to be solid, at least as far as seismic waves are concerned.

3. The core. This is the interior of the earth, starting at the centre and having a radius of 3470 kms. It is thought to be composed of iron and nickel in the free state, and furthermore, is thought to be in the fluid state, except for a small region in the centre known as the inner core. The reason for believing that it is in the fluid state is the fact that it will not sustain shear waves in the seismic frequency region.

Earthquakes have provided a great deal of information about the earth, but because of the inability of the seismologist to get the exact time and location of occurrence, there has always been a certain degree of uncertainty in the data derived regarding the crust of the earth. More recently, seismic equipment has become available with much higher resolution than the old seismometers used in earthquake measurements, and consequently controlled seismic experiments are now possible.

Seismic surveys of the long range type have only been carried out since about the early 1950's. The nature of these surveys has been to try and delineate the structure of the crust down to the Mohorovičić discontinuity. It was expected

that the crust would be composed of different layers, having different seismic properties, and as a consequence of this useful seismic reflection and refraction data could be obtained from these boundaries. The implementation of long range refraction surveys is relatively straightforward.

In general, one chooses an area in which one wishes to determine the crustal structure. After selection of the area, shot holes are drilled at both ends of the line of interest, and recording locations are interspersed at uniform distances between the shot points. At prearranged times, explosive charges (usually TNT or dynamite) are exploded in one of the two shot holes, the charges providing a source of energy for the propagation of elastic waves through the crust. These waves are reflected and refracted along the various boundaries of the crust, and return to the surface of the earth. At the recording locations, trucks equipped with instruments which are sensitive to ground motions (geophones) record these reflected and refracted arrivals. From the measured times of arrival of the waves, it is possible, using simple ray path methods, to determine the structure and velocity distribution of the crust. See fig. A for a diagram illustrating this method.

Such data are of fundamental importance to the seismologist. Long range surveys provide a good approximation

of the layered crustal structure, and where it is important, this layered structure may be interpreted in terms of the surface topography (e.g., under mountains one would expect there to be some deformation of the mantle at the Moho boundary which would reflect the fact that mountains exist above it). Furthermore, these data allow us to make certain deductions about the elastic properties of the crustal materials, what the form of these materials might be, and whether the boundaries in the crust represent sharp discontinuities or simply transition zones, which are perhaps only a wavelength or so wide. Refraction surveys carried out on a local scale cannot hope to answer such broad questions, but with the ever increasing amount of data, a more universal picture should become available to the geophysicist.

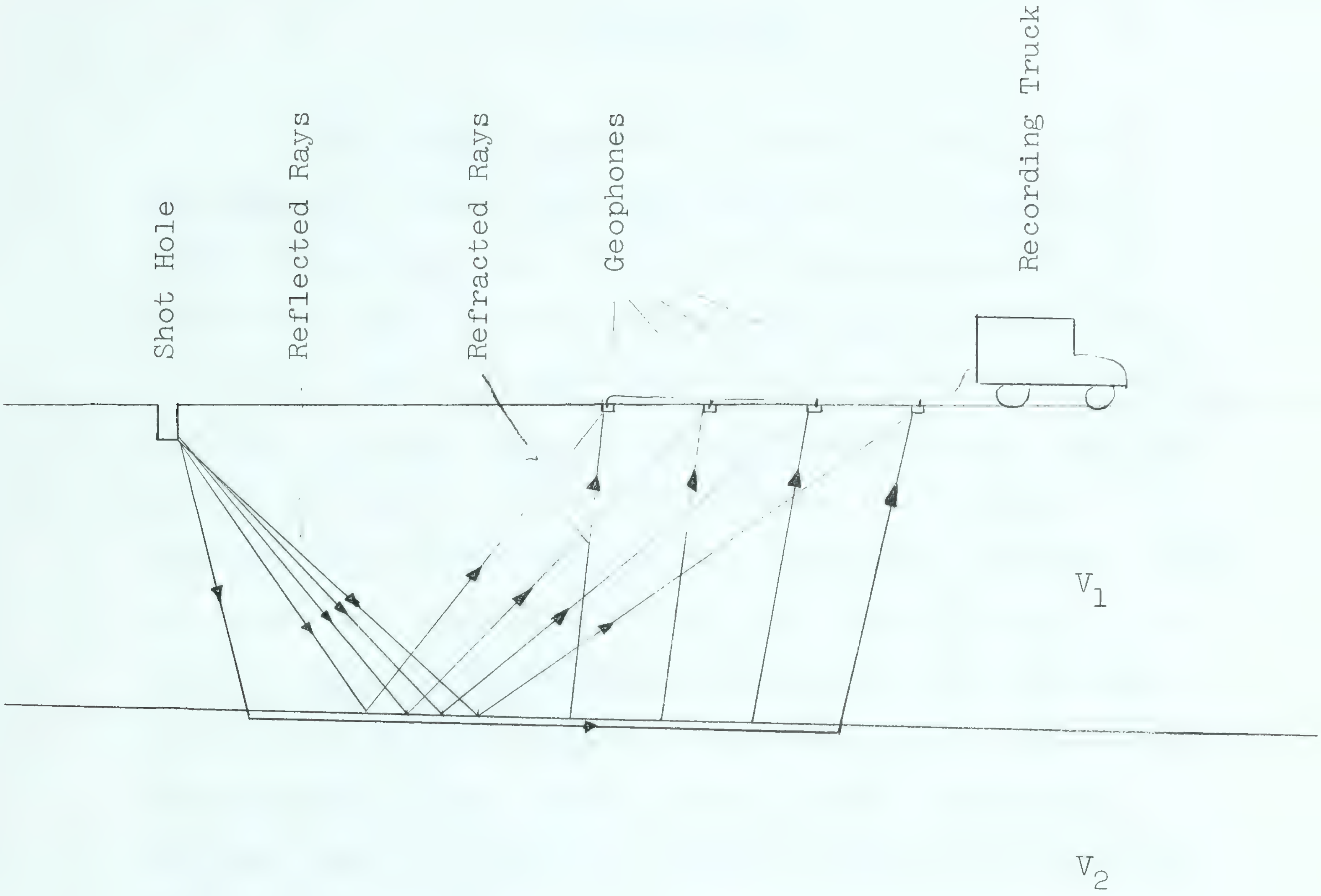

Fig. A. Simple Diagram to Illustrate Ray Path Propagation in a Layered Earth, and the Method of Recording.

Introduction

The present program of crustal studies at the University of Alberta had its inception in the summer of 1962. Since this time a number of experiments have been carried out and completed, among them being a double ended refraction profile between Suffield, Alberta and High River, Alberta, a double ended refraction profile between Suffield, Alberta and Swift Current, Saskatchewan, an extension of the Suffield data to the west out to a distance of 500 kms., and the start of a program to detect near vertical reflections from the deep crustal layers. Furthermore, the University took part in the Lake Superior experiment which was conducted in the month of July, 1963. Weaver (1962) has analyzed the data from the Suffield - High River profile and reports the following results:

Depths under the West Shot Point (Vulcan)

to Limestone (Miss.) = 1.70 kms
to Precambrian = 2.52 kms
to low velocity layer =22.52 kms
to Conrad =33.05 kms
to Moho =46.74 kms

Depths under the East Shot Point (Suffield)

to limestone (Miss.)	= 1.17 kms
to Precambrian	= 2.87 kms
to low velocity layer	= 22.87 kms
to Conrad	= 35.23 kms
to Moho	= 48.16 kms

The true velocities in each of these layers was as follows:

V_1 = 3.18 kms/sec

V_2 = 5.88 kms/sec

V_3 = 6.40 kms/sec

V_4 = 6.10 kms/sec (assumed)

V_5 = 7.32 kms/sec

V_6 = 8.25 kms/sec

Weaver was forced to contrive a low velocity layer in order to explain the fact that critical distance calculated from a straightforward interpretation of the refraction graphs was much greater than that actually observed. He does, however, present a good argument as to why there could indeed exist such a layer in southern Alberta; the reader is referred to Weaver (1962) for this argument.

During the summers of 1963 and 1964 a double-ended refraction profile was completed between Suffield, Alberta and Swift Current, Saskatchewan. A total of 30 records were obtained along this line, 17 from the east shot point (Swift Current) and 13 from the west shot point (Suffield). These records were plotted on reduced travel

time graphs, and in conjunction with three continuous velocity logs, a six layer earth model was postulated for the crustal structure in southern Saskatchewan. Some problems did arise in the interpretation of the data. These will be discussed in their appropriate section.

Most of the records along both lines were digitized, and the power spectra were computed for these records. It was found the spectrum of the records was closely related to the geologic environment of the shot holes. Furthermore, it was found that at least along the Suffield east line, there was little or no change in the frequency with distance.

A discussion of the Swift Current - Suffield line will comprise the bulk of this thesis. There will be a brief mention of the results of the westerly extension of the Suffield - High River line.

Chapter 1

1.1 Instrumentation.

Reference to figs. 1a and 1b shows the instrumentation system used at both the recording location and at the shot point. The recording location system is relatively simple. The signal from 12 different seismometers along the spread are fed into twelve separate VLF refraction amplifiers. The filtered, amplified signal is then fed into a recording oscillograph, and a paper record produced of the signal. As one can see, there are three auxiliary signals fed into the oscillograph. They are from a chronometer, a WWV receiver, and a standard broadcast receiver. These signals were reproduced in order to facilitate the timing of the spread location records.

The recording system at the shot point is even more simple. The shot instant from the shooting box, the signals from a chronometer, a WWV receiver, and a standard broadcast receiver are all fed into a recording oscillograph, and a paper record produced of these signals. This record is used to mark the shot instant onto the spread records.

This system was used for most of the work which is discussed in this thesis. During the spring of 1964, however, the VLF amplifiers were modified in order to increase sensitivity and improve signal to noise ratio. At the same time, outputs were provided for tape recording. A few records were made using this modified system.

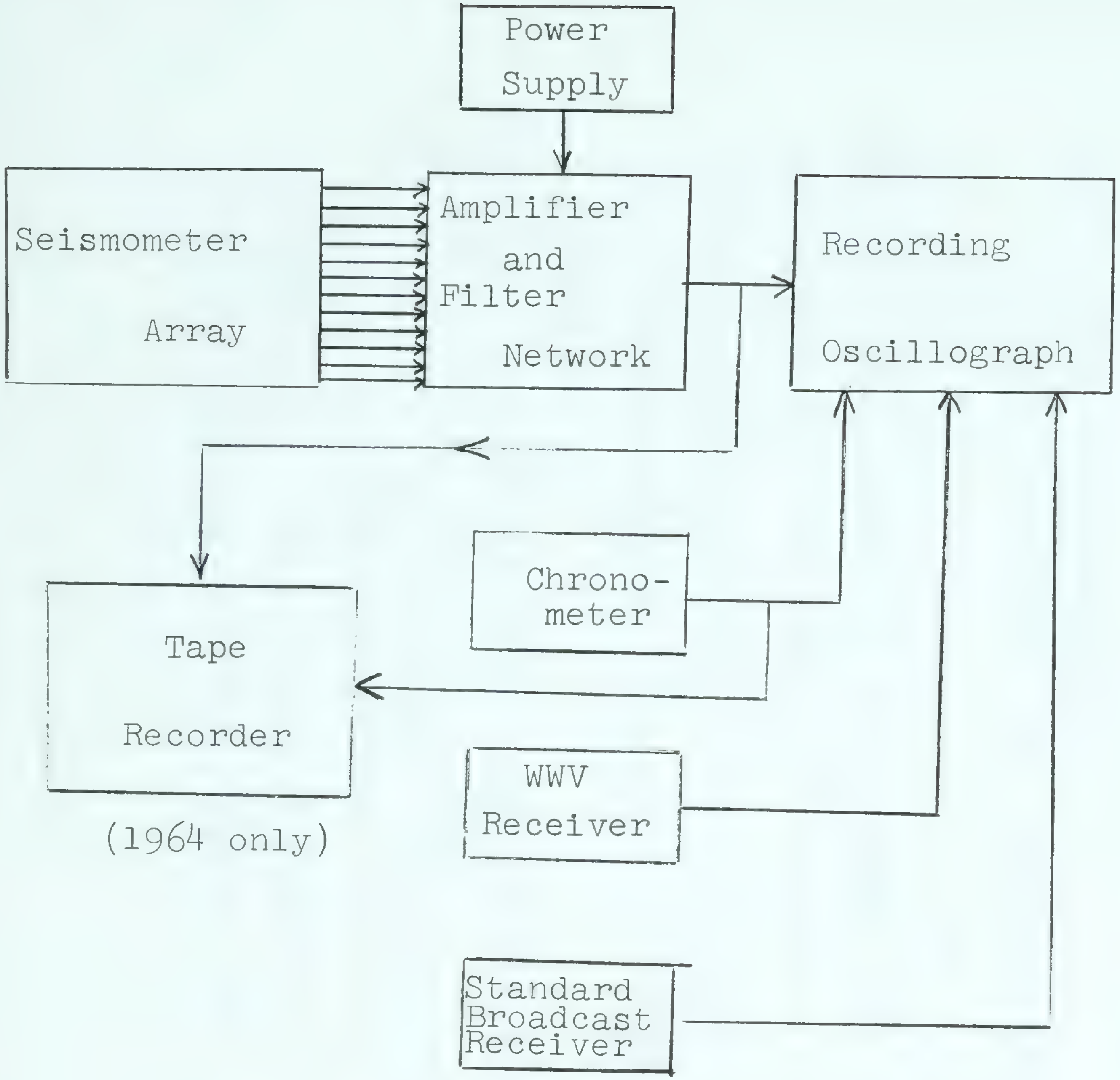

Fig. 1 a. Block diagram of Instrumentation System used in Recording Trucks.

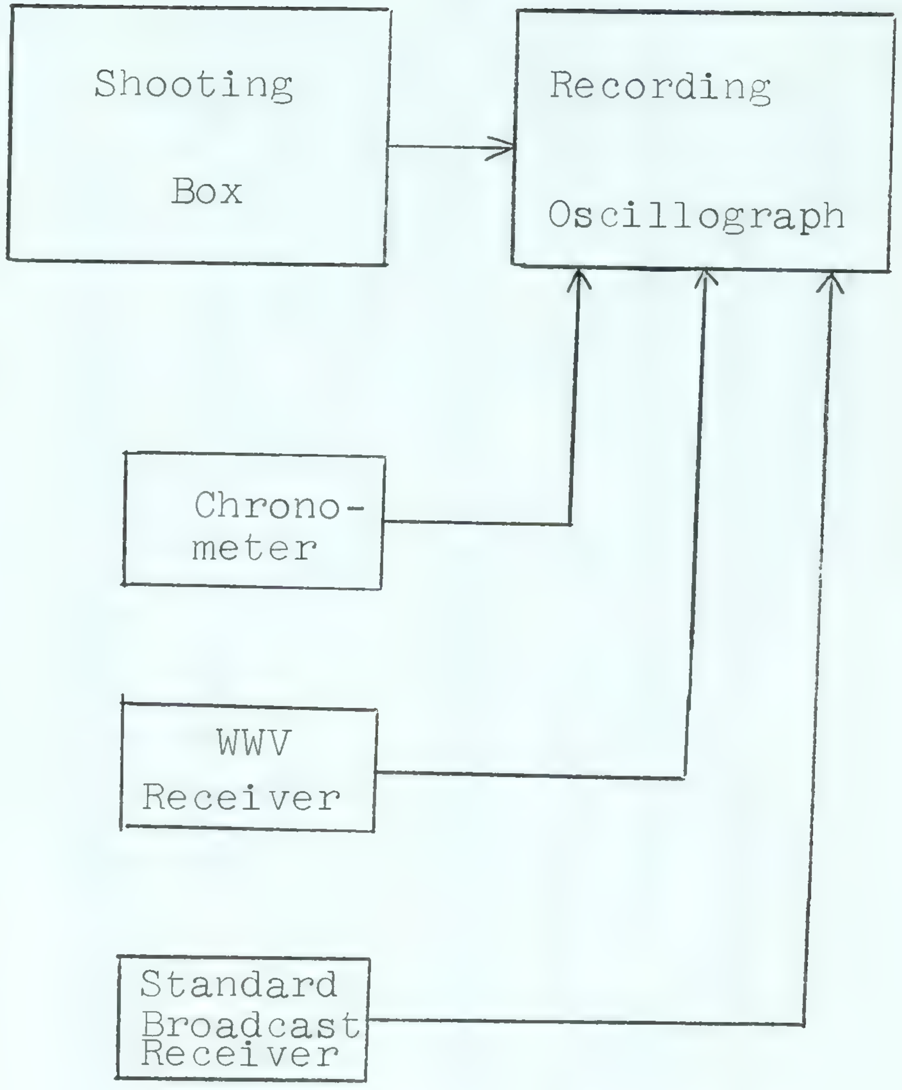

Fig. 1 b. Block diagram of Instrumentation System used at the Shot Point.

1.11 TIS-36 Seismometer.

The Texas Instruments S-36 seismometer was used for most of the geophysical measurements carried out at the University of Alberta. Its characteristics are as follows:

(a) The detector has a double coil system wound as a "hum bucking" device.

(b) The natural frequency is 2 cps ± .05 cps.

(c) The coil resistance is 4000 ohms.

The frequency response characteristics are shown in fig. 2.

1.12 VLF Refraction Amplifier.

Texas Instruments VLF refraction amplifiers have been used throughout the operations. The total drain of the 100 V power supply is 55 milliamps. The system performance figures for the unmodified amplifiers are as follows:

(a) The frequency response is 0.7 to 33 cps. Fig. 3 shows the system response curves for six different filter settings.

(b) Fig. 4. gives the phase response curves in milliseconds.

(c) Distortion is below 1% at 7 cps, for inputs below 2 millivolts, with the gain adjusted to give a 1" peak-to-peak deflection. Fig. 5 shows the variation of distortion with input under the conditions stated above.

(d) For an input of 15 microvolts, zero db. attenuation and the high cut filter set at 48 cps, the deflection of the high gain trace is 1" peak-to-peak. See Fig. 6 for overall magnification of system, including geophones.

(e) The input impedance is 10,000 ohms, and the line is balanced. No input transformer is used.

(f) The internal instrument noise is equivalent to an input signal of 3 microvolts.

(g) There are dual outputs, having a deflection ratio of 4 to 1. No output transformer is used; one side of the output line is grounded.

The external features of the system are as follows:

(a) There are two input plugs, having precisely reversed polarities.

(b) Switching facilities include a line test switch to check the continuity of the spread line, separate attenuation switches for each amplifier (calibrated in 6 db. steps), 1 filter setting switch for each pair of amplifiers (calibrated with positions at 8, 12, 16, 24, 32, and 48 cps), and line balancing switches for each amplifier which simply introduce resistive line balancing to create a common mode rejection of 60 cps signals induced by nearby power lines.

The modified amplifiers have the following added features:

(a) The gain has been increased by a factor of 15.

(b) Input transformers are now used, maintaining an input impedance of 10,000 ohms.

(c) The line balancing circuit has been modified in its circuitry, but it still performs the same operation.

There have been further radical changes in the internal circuitry of the amplifiers. These modifications were made in an effort to enhance the gain of the system and to enhance the signal to noise ratio. It appears that these modifications have been eminently successful.

1.13 Power Supply.

The power supply is a fairly standard unit, delivering 100+ volts DC. A 12 volt dc input is inverted to a.c. by a transistorized inverter, amplified, then rectified and filtered to give an output of 300 volts dc. This voltage is then passed through a tube type regulator, which finally delivers 100 + volts of well regulated dc. This voltage may be adjusted to suit the operating condition of the amplifiers.

This power supply was also modified to fit the new system of amplifiers. The output was broken up into three separate outputs. Regulation of two of the outputs is performed by the standard voltage-regulator tube circuit, while the critical reference voltage for the amplifiers is now

set by a 97 volt battery pack, rather than by V-R tube regulators. These voltages are not adjustable by an exterior control.

1.14 Recording Oscillograph.

The RS-8U recording oscillograph is a self contained unit composed of an optical system, a timing system, recording galvanometers, and a paper transport system. Its characteristics are,

(a) Some 30 galvanometers having a natural period of 200 cps.

(b) Three paper speeds are available: slow, medium, and fast, corresponding to speeds of about 2, 4, and 10 inches per second.

(c) Timing lines are provided by a 100 cps transistor supply and a synchronous motor driving a drum containing slits.

(d) There are 24 channels of seismic information possible, 12 being the high gain traces and the other 12 being the low gain traces. Deflections are in the ratio of 4 to 1. There are some six other auxiliary channels.

(e) The intensity of the recording lamps is governed by the paper speed switch, being brightest for high speed, and dimmest for low speed.

(f) The paper transport system handles a roll of seismic photographic recording paper which is 8" x 200'.

(g) Fixing and developing of the records is accomplished in the tanks fitted below the camera in a light tight box.

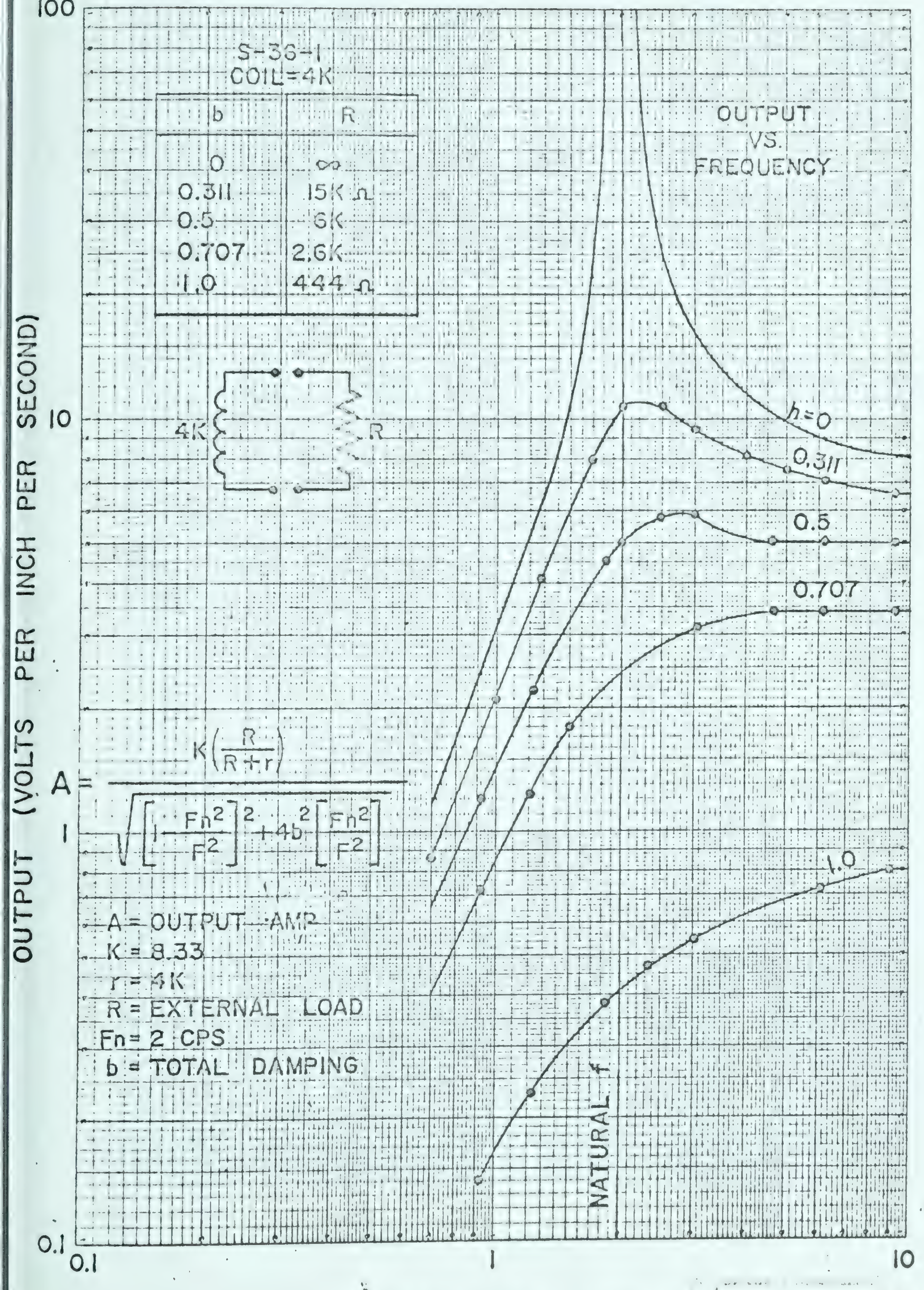
100
10
1
0.1
0.1
1
10
S-36-1
COIL=4K
b
R
0
∞
0.311
15K Ω
0.5
6K
0.707
2.6K
1.0
444 Ω
OUTPUT
VS.
FREQUENCY
4K
R
h=0
0.311
0.5
0.707
1.0
NATURAL f
$A = \frac{K\left(\frac{R}{R+r}\right)}{\sqrt{\left[1-\frac{Fn^2}{F^2}\right]^2+4b^2\left[\frac{Fn^2}{F^2}\right]}}$
A = OUTPUT AMP
K = 8.33
r = 4K
R = EXTERNAL LOAD
Fn = 2 CPS
b = TOTAL DAMPING
OUTPUT (VOLTS PER INCH PER SECOND)
FREQUENCY (CPS)

Fig. 2

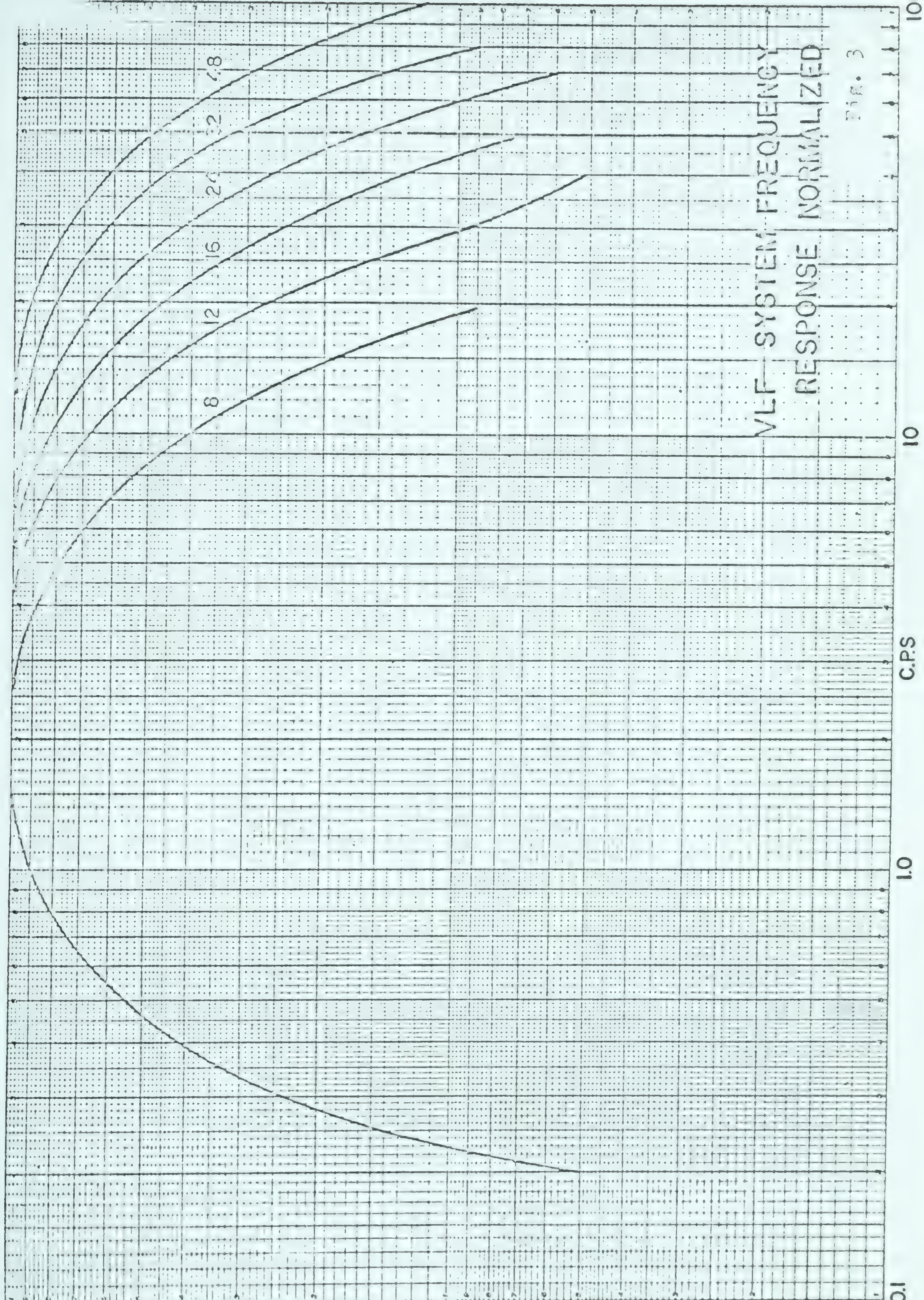

VLF SYSTEM FREQUENCY RESPONSE NORMALIZED

Fig. 3

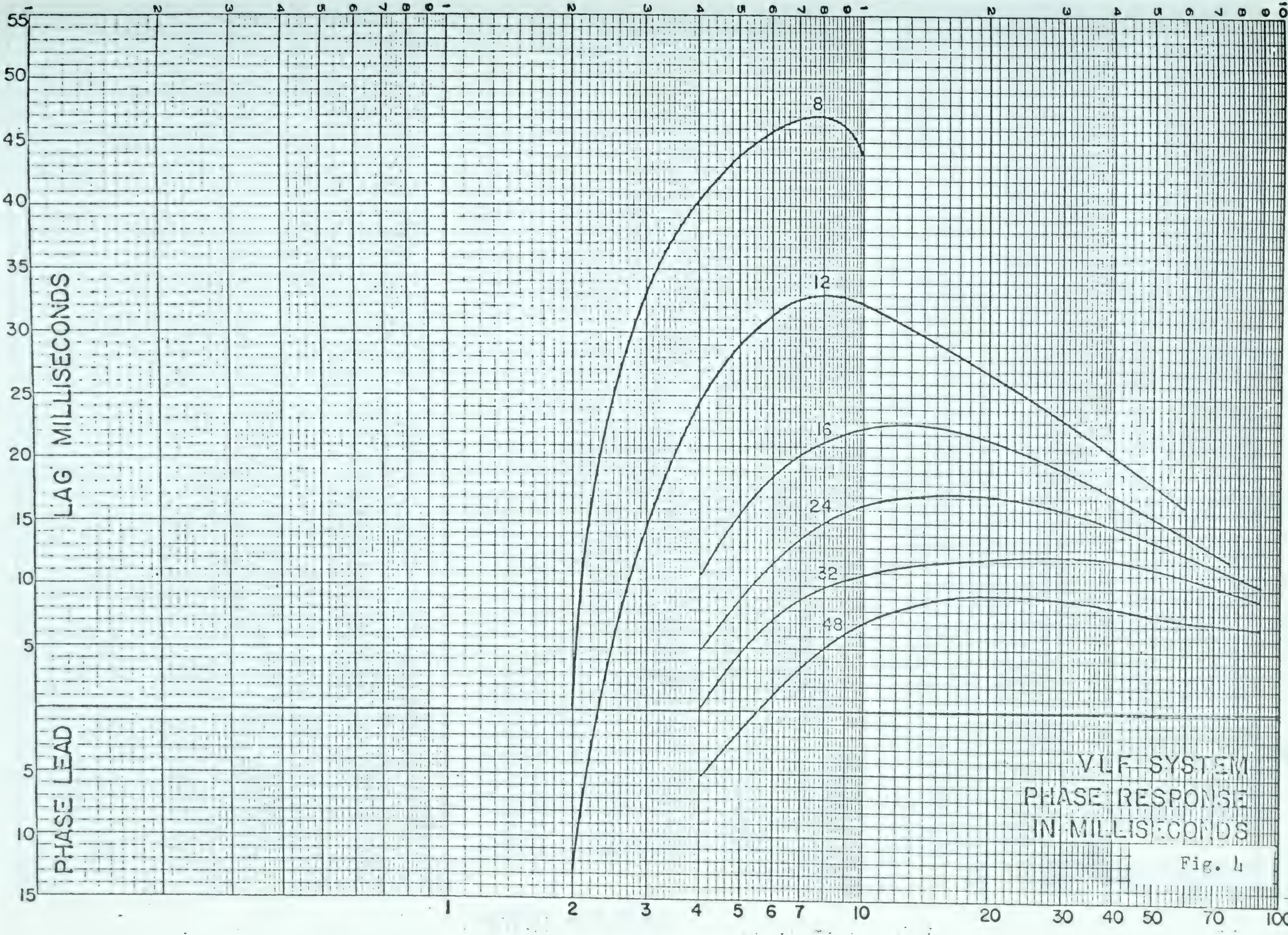

VLF SYSTEM
PHASE RESPONSE
IN MILLISECONDS

Fig. 4

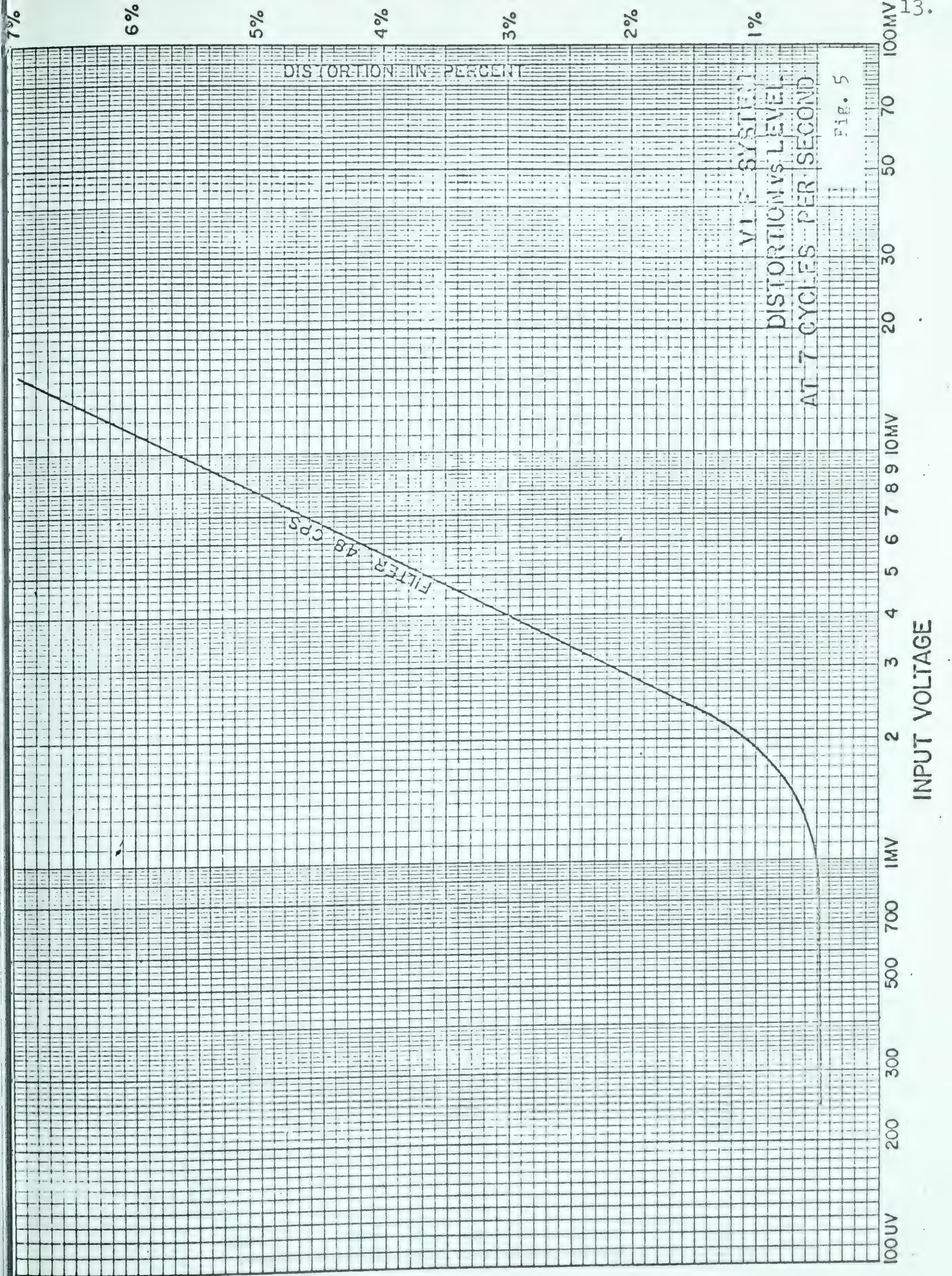

VLF SYSTEM
DISTORTION VS LEVEL
AT 7 CYCLES PER SECOND

Fig. 5

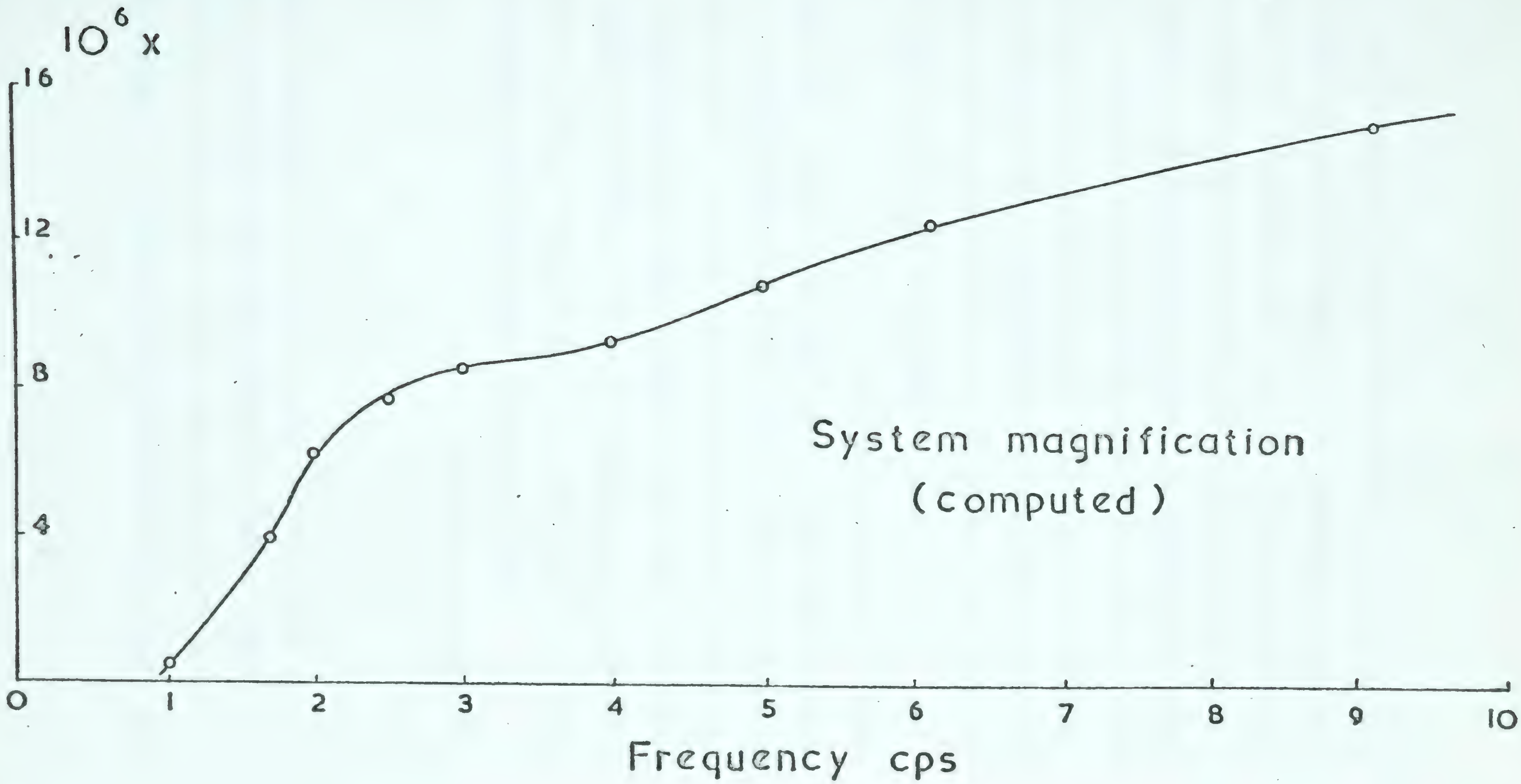
10^6 x
16
12
8
4
0
1
2
3
4
5
6
7
8
9
10
Frequency cps
System magnification
(computed)

Fig. 6

(h) Power requirements are 12 volts dc. Dissipation is at the rate of 13 amps during recording at the highest speed. The timing system draws 0.150 amps. The RS-8U camera was not modified for the new system of amplifiers.

1.2 Field Procedure.

The trucks were fitted with the following equipment: one 12 channel TI VLF refraction amplifier and associated power supplies, a recording oscillograph and its associated developing tanks, a Westrex chronometer, a WWV receiver, a standard broadcast receiver, 13 TI S-36 geophones, two geophone cable reels (each holding one mile of cable), assorted shovels, a tool box, spare paper, and additional cans of developer and fixer.

The field procedures adopted were fairly simple, calling for a maximization in time saving and a minimization in energy expenditure. Recording locations were usually chosen during planning sessions conducted in Edmonton. They were chosen with the following criteria in mind: first, that each recording location should lie on, or very close to the straight line which joined the two shot points (i.e. Suffield and Swift Current), and secondly, that these recording locations, when viewed as a whole, should give fairly uniform coverage along the refraction line.

Once we had actually arrived at the recording location specified for the days shooting, we checked the location for power lines. If there were any, we usually drove a mile or two north or south of this location in order to find a location free of power lines. In general, it was possible to find such a location. Having arrived at a suitable location we proceeded to lay out the geophone cables.

Laying out of the cable was performed as follows: one cable reel was placed at the back of the truck, and while one crew member drove slowly along the road, the other guided the cable into the ditch at the edge of the road. As each geophone takeout was reached, a seismometer was taken from the truck, unclamped, and dug into the ground at this location, such that its top was just flush with the surface of the ground. It was found that this gave the maximum signal to noise ratio. It should be noted that 40 feet of slack cable was paid out at the beginning. This was done to ensure that the spacing between geophones 6 and 7 was consistent with the spacing of the other geophones. This same procedure was followed for the other cable. Having laid out both cables, the truck was driven back to the center of the spread and pre-shot checks were begun.

After the cables were plugged into the amplifier bank, the line test switch was used to test the continuity of the line. If the resistances on each geophone were found to be in the range of 2700 to 3500 ohms, they were considered to be all right. If the resistance was infinite, this usually implied an improper connection, and it was then checked by one of the crew members. A geophone whose resistance was too low was checked first for a shorted connection, and if this was not the cause, then the instrument was replaced by the spare. Having completed the continuity check, the next problem was to set the chronometer.

Using WWV as our time signal, the chronometer was started, then set against this time signal by means of a manual control. A short record was then made of the WWV signal and the chronometer marks on the recording camera. This record sufficed to calculate the error in the chronometer against WWV . Absolute time could now be read off the record of the chronometer marks to an accuracy of about ± 5 milliseconds.

The amplifiers were now switched on, and the traces of the seismometers observed. The ambient noise level tolerable was a deflection of up to 1/4" on the high gain traces. Normal operational settings of the external switches were 16 cps high cut filter, and either 0 or 6 db. attenuation. Line balancing was always used. With the modification of the

amplifiers, the normal high cut has been increased to 24 cps, and the normal attenuation is 18 db. or greater. This figure is the lowest yet used, and this was at an exceptionally quiet location.

The system was then shut down until about 5 minutes before shot time. At this time, all instruments were started again. The WWV receiver signal was observed on the camera, the standard broadcast receiver was set to a pre-arranged broadcast station and its filtered, rectified signal observed on the camera, the chronometer (which remains running until the end of the operation) was rechecked against WWV, and the ambient noise level was rechecked. Any adjustments to the various filter and attenuation settings were made at this time and were considered to be final. At about five seconds before the shot time, the camera was switched on, and a record of ground motion was made until 2 minutes after the pre-arranged shot time. The record was then developed, washed, fixed, rewashed and then examined for arrivals if they were not visible on the galvanometer bank during actual recording. It was then labeled with appropriate information as to shot time, location, date, filter settings, attenuation, etc. The instruments were now shut down, the galvanometer bank reclamped, the lids put back on the developing cans, the cables unplugged, and antennae were taken down. We then

drove to either end of the line, backed up the line, with one crew member sitting in the back of the truck reeling in the cable, stopping at each geophone location to pick up the instrument, clamp it and replace it in the box in the truck. When both cables were picked up, they were fixed in the back of the truck, tied down (in order to keep them from moving too far in case of an accident). All the other loose gear was then packed into the van, and we were ready to proceed to the next location.

1.3 Spread Locations and Shot Information.

Fig. 7 is a map of southern Alberta and southwestern Saskatchewan. The dashes indicate the spread locations, and are drawn approximately to scale (spread lengths were 2 miles). There are some 13 records recorded from the Suffield shot point, and 17 records made from the Swift Current shot point. Those spread locations west of Suffield were recorded from the Swift Current shots. This extension was made in order to obtain first arrival information of the P_n refraction.

There is a gap in the middle of the line. This gap is located in the Great Sand Hills of southern Saskatchewan. We felt that since map coverage was poor in this area, and the surface material was sand, it would not afford a good recording location. Subsequent perusal of the area confirmed our suspicions.

Table 1 gives information regarding shot dates, time, distance from the shot point, and size of the shot.

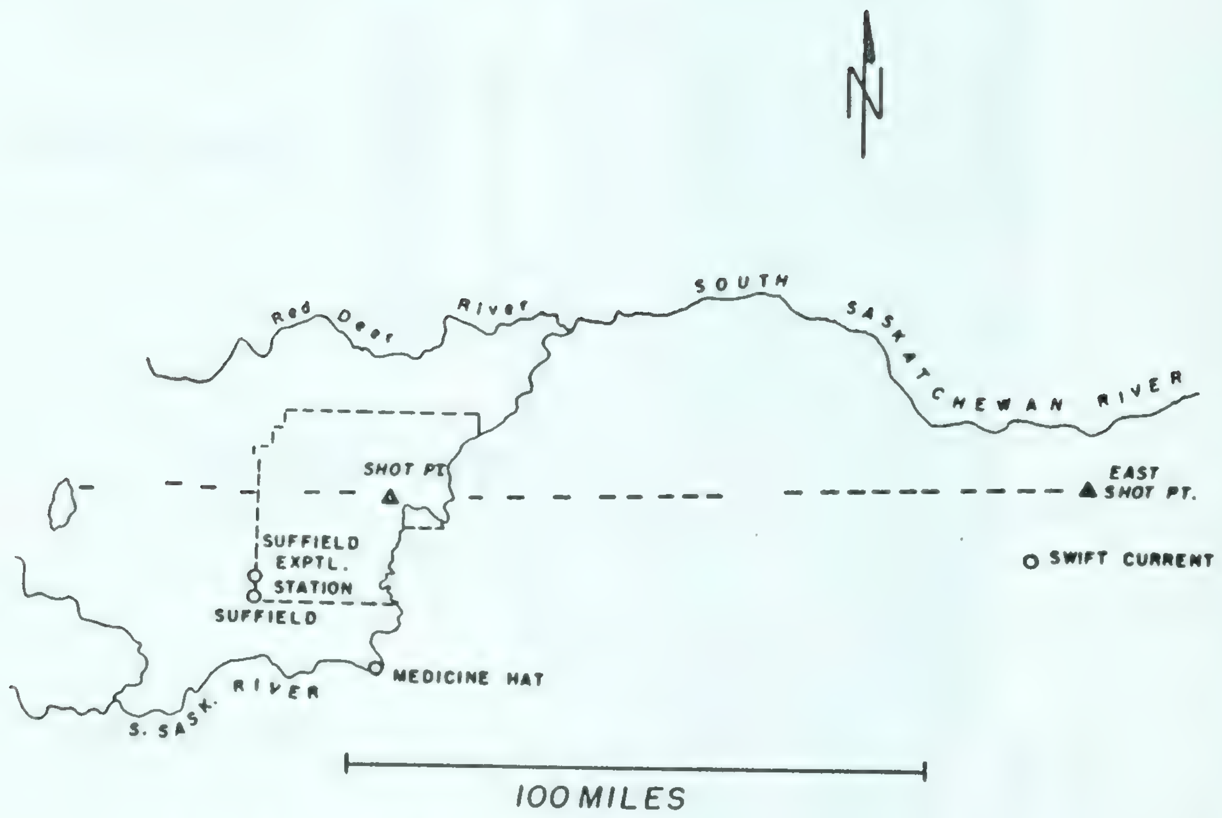

SHOT POINT AND SPREAD LOCATIONS
UNIVERSITY OF ALBERTA
REFRACTION PROFILE
- *Spread locations*

Fig. 7

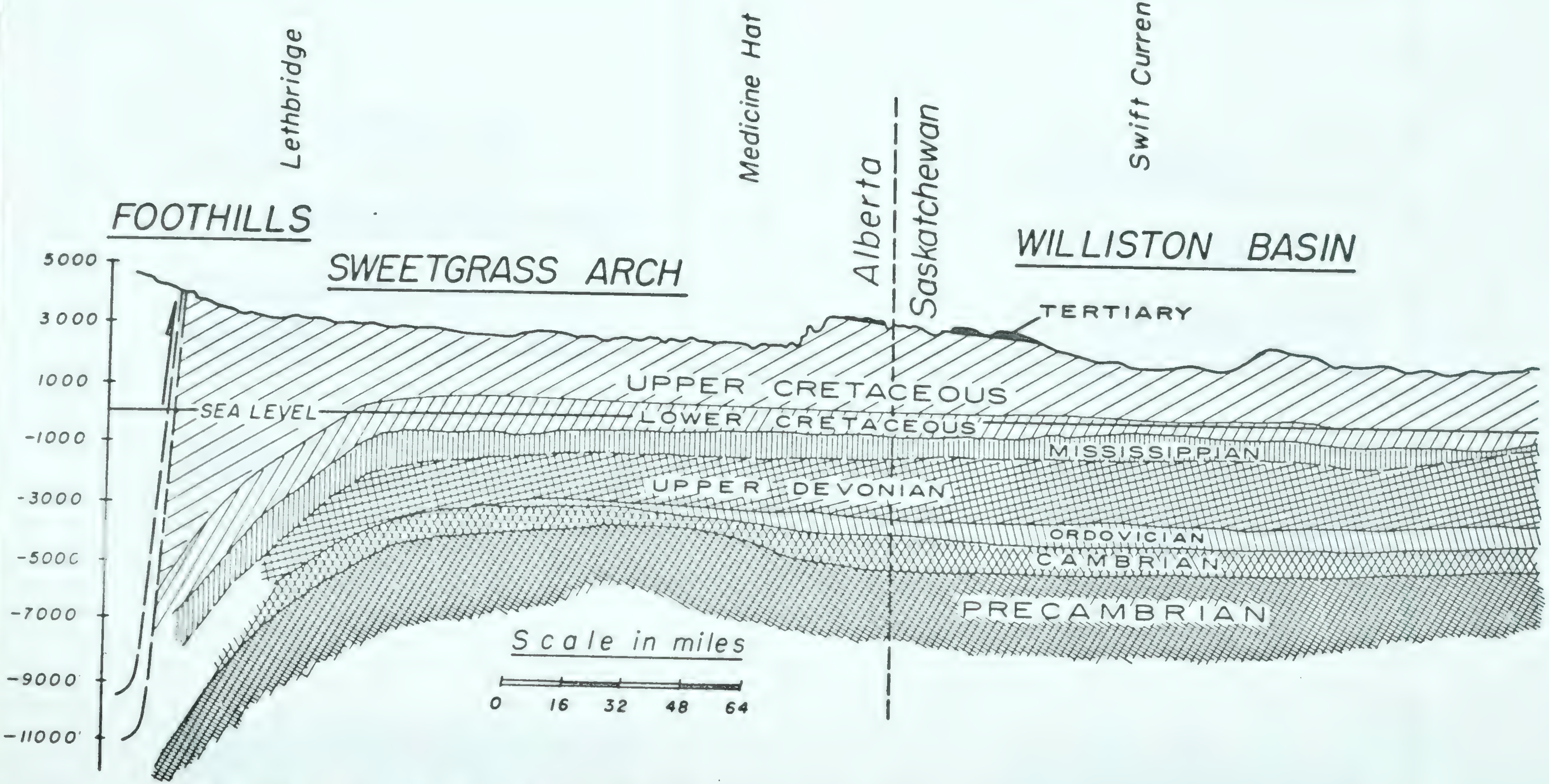

Southern Alberta - Saskatchewan regional cross section

Suffield East Profile.

Spread No.	Shot Date and Hour	Distance (kms)	Shot Size (lbs)
1	9 8 63 10.00	77.28	1000
2	9 8 63 10.00	89.28	1000
3	9 9 63 10.00	127.67	1000
4	9 9 63 10.00	134.19	1000
5	9 9 63 15.15	135.82	1000
6	9 10 63 10.00	155.33	1000
7	9 10 63 15.00	165.18	1000
8	9 10 63 10.00	169.94	1000
9	9 10 63 15.00	181.52	1000
10	9 11 63 10.00	193.52	1000
11	9 11 63 15.00	201.35	1000
12	9 11 63 10.00	205.76	1000
13	9 11 63 15.00	213.89	1000

Swift Current West Profile.

Spread No.	Shot Date and Hour	Distance (kms)	Shot Size (lbs)
14	8 3 64 10.00	19.52	400
15	9 12 63 10.00	32.58	200
16	8 13 64 10.00	47.16	400
17	9 12 63 15.00	63.31	200
18	9 12 63 10.00	86.19	200
19	9 12 63 15.00	113.84	200
20	6 16 63 19.00	138.23	425
21	6 16 63 11.00	149.71	625
22	9 13 63 10.00	164.25	500
23	6 15 63 19.00	213.02	1000
24	7 26 64 19.00	227.84	600
25	9 13 63 10.00	236.86	500
26	7 26 64 19.00	253.04	600
27	7 25 64 19.00	263.47	800
28	7 25 64 19.00	268.16	800
29	7 24 64 19.00	285.06	800
30	7 24 64 19.00	300.97	800

Table 1

Chapter 2.

2.1 Power Spectral Analyses.

Some seven records from the Suffield East line were analyzed, while fourteen records from the Swift Current West line were analyzed. In this thesis, however, only the seven spectral analyses of the Suffield data are shown in fig. 8 and three of the Swift Current spectral analyses in fig. 9. The reason for the large number of Suffield records is that they were considered to comprise the most uniform group of data; the shot size remained constant at 1000 lbs. and the shot holes were only used once. The Swift Current data, however, are not nearly so uniform. The shot size varied in most cases, and often the same shot hole was used more than once.

The computational techniques are described in Appendix 1, but it might be instructive to describe the method used in digitizing. All the records were digitized by hand. The section digitized in every case consisted of that part of the record from about 200 msecs. before the first arrival to about 5 to 7 seconds after the first arrival. The digitizing interval was 10 msecs. Care was taken to insure that the records were lain flat, so that only linear trends were introduced into the data; such

trends being removed by the computer program before actual spectral analysis was begun. Only the first 5 to 7 secs. was digitized because nearly all of the information of interest was contained in this part of the record.

2.11 Power Spectra of Some Suffield Records.

Fig. 8 illustrates the Suffield power spectra. There are some important points in regard to these data. The most important is the fact that there appears to be little or no change in frequency of the main peak (5 cps) with distance from the shot point. This is not expected since according to the theory of wave propagation in layered media, there should be an attendant attenuation of high frequency signal with distance from the shot point (McDonal, Angona et al (1958), Ricker (1944), Kovach, Lehner and Miller (1963)). We note that any fine structure in the peaks is real, since the relative noise level is some 2 or 3 magnitudes lower than the main peak.

The next most important feature of this set of data is the fact that the main band of energy transmission is 5 cps, an unusually low frequency for such close-in refraction work. A more normal frequency is considered to be about 10 cps. We note in the diagram that the geologic environment of the shot holes is a heavy glacial boulder till, overlying arenaceous Cretaceous beds (Jones, 1963). The

boulder till is also riddled with gravel lenses. This type of shot hole environment will attenuate the high frequency of the outgoing explosive pulse, such that only very low frequencies remain. The resulting records have a very "loopy" appearance, and correlation from record to record is very difficult since there is virtually no character to the record (Dr. E. R. Kanasewich, personal communication and Mr. W. G. Smith, personal communication). This last fact probably accounts for the major uncertainties of the proposed crustal structure, since the Suffield travel time graph is not considered to be as reliable as the reverse profile.

It is interesting to note that there appears to be a peak at about 10 cps, which, on the average, seems to diminish with distance. This is misleading, however, since this peak is not real in all cases, on some records being signal, while on others it is noise. This can easily be seen on the original records by noting the presence or absence of 10 cps energy before the first arrival.

Although no data past 25 cps are shown, spectral calculations were carried out to 50 cps. On some of the power spectra calculated there appeared to be a strong peak at 40 cps: we consider this to be due to aliasing of a 60 cps signal which is sometimes evident on these records.

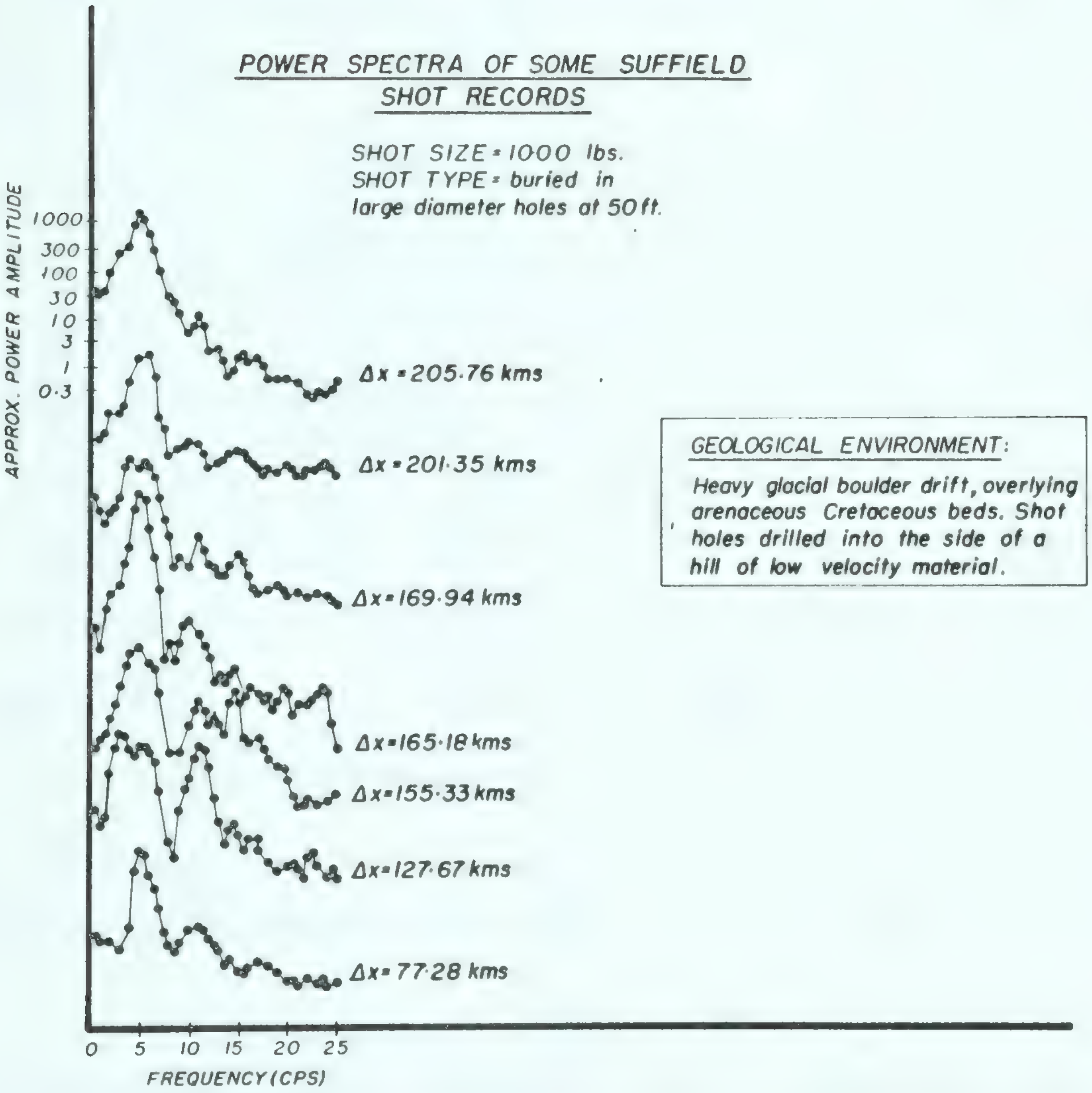
POWER SPECTRA OF SOME SUFFIELD SHOT RECORDS
SHOT SIZE = 1000 lbs.
SHOT TYPE = buried in large diameter holes at 50 ft.
GEOLOGICAL ENVIRONMENT:
Heavy glacial boulder drift, overlying arenaceous Cretaceous beds. Shot holes drilled into the side of a hill of low velocity material.
APPROX. POWER AMPLITUDE
1000
300
100
30
10
3
1
0·3
Δx = 205·76 kms
Δx = 201·35 kms
Δx = 169·94 kms
Δx = 165·18 kms
Δx = 155·33 kms
Δx = 127·67 kms
Δx = 77·28 kms
0
5
10
15
20
25
FREQUENCY (CPS)

Fig. 8

2.12 Power Spectra of Some Swift Current Records.

Fig. 9 illustrates some Swift Current power spectra. It is immediately evident that the power spectra are much more complicated for this series of shots. Perhaps we should first note that the noise is some two or three magnitudes lower than the signal.

The most important feature of this set of data is the fact that the high frequency content has not been attenuated as in the Suffield records. This is due in main to the shot hole environment. The holes were drilled into a blue clay horizon of the Upper Cretaceous. This being a fairly compacted medium, with a velocity of about 6,000 ft/sec, high frequency data is transmitted quite readily. We should note that shots number 17 and 23 were shot in holes used for a second time: there appears to be little attenuation of high frequency data, even though one would expect this to occur since the shot holes would be brecciated.

If one examines the highest peak of the three records presented, there appears to be a frequency shift downward, as the distance from the shot point is increased. Whether this is due to attenuation of high frequency with distance, or to an increase in shot size, is not possible to determine with the present set of data. Further work, with a more uniform set of data, is required.

Another important point to note in these records is the multiplicity of peaks which are visible on the main peak. Interference of two seismic pulses may be the cause of these peaks or, as is more likely, they are a reflection of the fact that waves travelling along different paths would tend to have different frequencies due to differences in path length. Visible examination of the records tends to bear out this latter statement. The first break (considered in most cases to come from the sub-basement refractor), has a frequency of anywhere from 10 to 12 cps, while the head wave from the Moho appears to have a frequency of about 8 to 10 cps. See P. S. Veitsman (1957).

As opposed to the Suffield records, the seismic records from Swift Current have very well defined character, especially in the case of the M refraction. Correlation by character is quite possible in many cases, and the phase velocities of most correlative arrivals have not been interfered with as a result of the low frequency character so evident in the Suffield records. If one accepts correlations made on such a basis, then we must accept the Swift Current travel-time graph as being well defined.

We conclude, then, by stating that the frequency spectrum of the two sets of data are very much dependent on the shot hole location. In the case of the Suffield shots,

EXAMPLES OF POWER SPECTRA FROM SWIFT CURRENT SHOT RECORDS

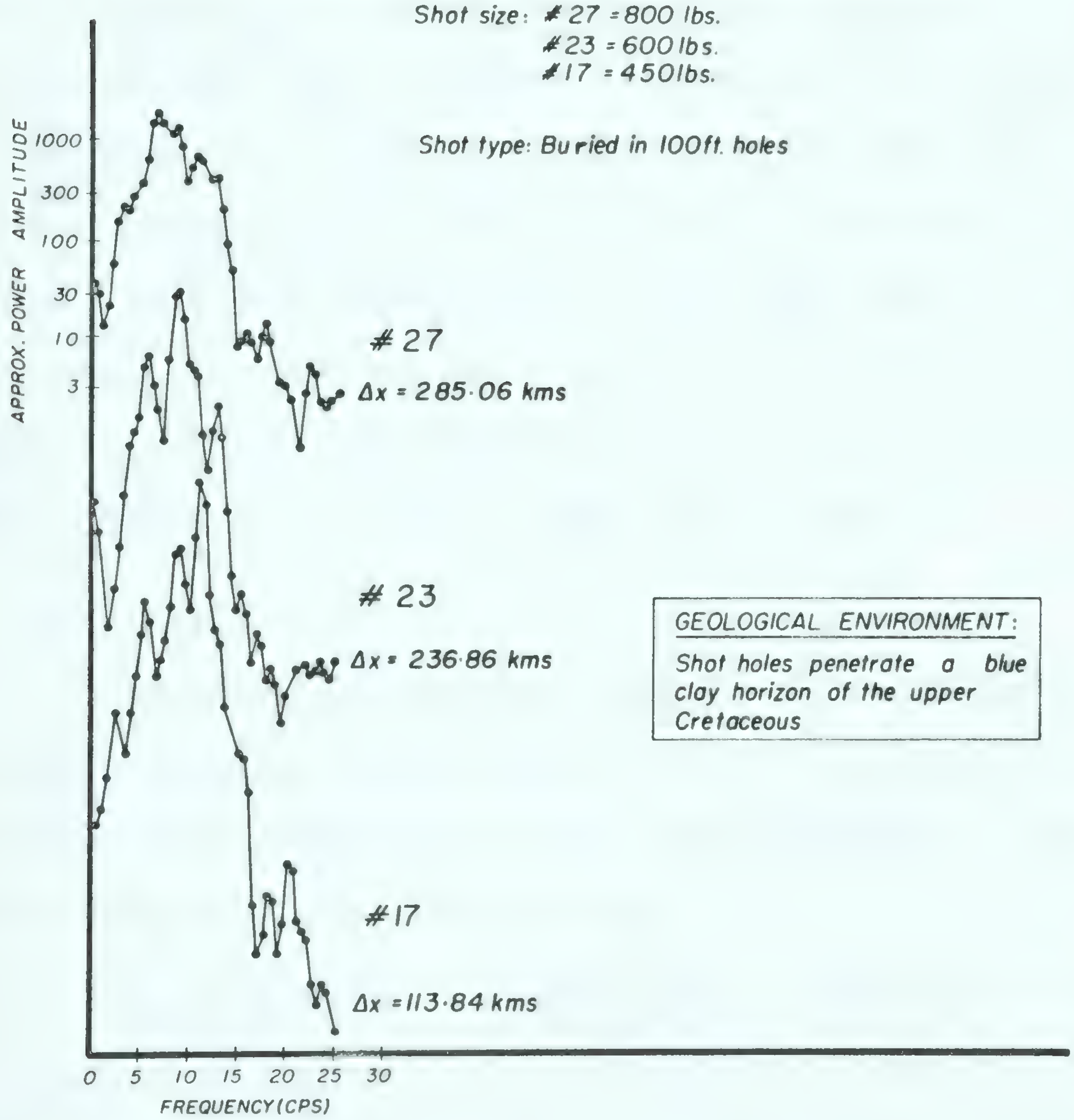

. Fig. 9

the spectrum consisted of one peak at about 5 cps, with little or no change in frequency with distance. This was presumably a result of the shot holes being in a low velocity, unconsolidated medium. The Swift Current records, on the other hand, have a spectrum which has clearly defined peaks out to a frequency of about 12 cps. There appears to be a shift in the main peak to lower frequencies with distance from the shot point, but it is not known whether this is due to a change in shot size or is due to attenuation with distance. The fact that there is more high frequency data in the spectrum reflects the fact that the shot holes were drilled into a blue clay horizon, which is a fairly consolidated medium, having a velocity of about 6000 ft/sec.

2.13 Amplitudes.

Although not directly related to power spectra, one should examine the records to see if there are any trends associated with amplitudes of the first arrivals. A plot of this data is to be found in fig. 10.

As is evident from this graph, there is quite a large amount of scatter in the experimental results. The points 1 and 3 are the only pair of measurements corresponding to records from the same shot. There is a marked attenuation of amplitude with distance noted in these points, but since other pairs of records could not be plotted, it is impossible

to draw any conclusions from such fragmentary evidence. We see that standard inverse square and inverse cubic curves (constrained to pass through point 1) do not fit the data at all well. In fact, there is very little pattern which emerges from this curve.

The reasons for this lack of pattern are perhaps two-fold. It is felt that the shot hole location and recording locations are responsible for this lack of coherency. As we pointed out earlier, this set of data is the most uniform set. This was evident even in the craters formed by the shots: their diameters varied only some 3 feet in 30 feet. Although this appears insignificant, if one considers the volume of such a crater (assuming spherical symmetry), variations of 3 feet in 30 feet correspond to variations of about 30% in the volume. There would be a concurrent loss in energy in such a shot; we feel that such large differences in the outgoing pulse energy would account to a large extent for the scatter in the amplitude measurements. Furthermore, variations could be expected in the geophone-to-ground coupling from location to location. Differences in the surface low velocity layer thickness would also account for differences in amplitudes.

To sum up, the scatter in the data is thought to result from two sources. They are loss of energy as a result of brecciation of the shot hole and loss of energy due to variations in the low velocity layer thickness and geophone-to-ground coupling.

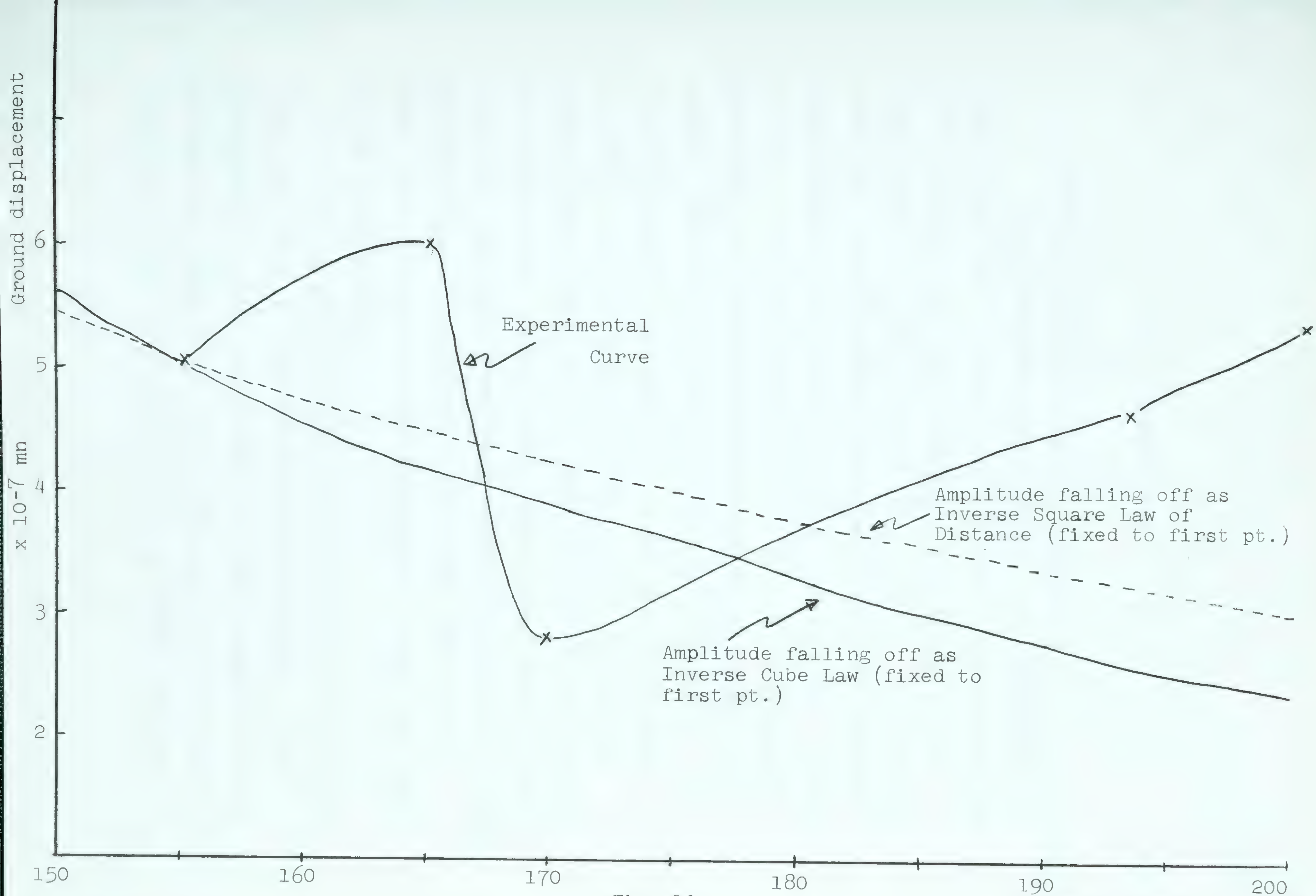
Ground displacement
x 10-7 mn
6
5
4
3
2
150
160
170
180
190
200
Distance (kms)
Experimental Curve
Amplitude falling off as Inverse Square Law of Distance (fixed to first pt.)
Amplitude falling off as Inverse Cube Law (fixed to first pt.)

Fig. 10

Chapter 3

3.1 The Post Precambrian Surface Structure.

From the travel time graphs of the experimental data we were able to deduce four separate refracting horizons. Well velocity logs, kindly supplied to us by the British American Oil Co., Ltd., enabled us to draw up a reasonable model for the near surface structure. These logs defined quite clearly three distinct velocity distributions, a low velocity surface layer consisting of all post-Mississippian sediments, the high velocity Mississippian limestone, and another low velocity horizon, the Cambrian sediments. In order to simplify our model, it was decided that lumping in the low velocity Cambrian sediments with the surface material would not affect our model, and would leave us with two layers at the surface rather than three. Figs. 11 and 12 illustrate the post Precambrian surface structure at Suffield and Swift Current as derived from the well logs, while Figs. 13 and 14 show the modified models of these logs used in our calculations.

It is perhaps important to point out at this stage that these velocity logs served a further purpose. The experimental travel-time curves were quite complete in their information regarding all three refractors below the Precambrian surface, but control of the P_g arrival from the

Low Velocity Layer
$\Delta z = .874$ kms.
V = 2.51 kms/sec.

2864' t = .348 secs.

Mississippian Horizon.
$\Delta z = .839$ kms.
V = 5.12 kms/sec

5615' t = .512 secs.

Cambrian Sediments
$\Delta z = .427$ kms. V = 3.81 kms/sec.

7015' t = .624 secs.

Precambrian V = 6.00 kms/sec.
(Assumed)

Fig. 11. Post Precambrian surface structure as defined by continuous sonic velocity logs. Suffield Shot Point.
one way reflection tim

Low Velocity Layer
$\Delta z = 1.138$ kms
V = 2.34 kms/sec

3730' t = .486 secs.

Mississippian Horizon.
$\Delta z = .755$ kms.
V = 5.32 kms/sec

6207' t = .628 secs.

Cambrian Sediments
$\Delta z = .126$ kms. V = 2.42 kms/sec.

6619' t = .680 secs.

Precambrian V = 6.00 kms/sec.
(Assumed)

Fig. 12. Post Precambrian Surface Structure at Swift Current as defined by Continuous Sonic Velocity Logs.
t = one way reflectio

Low Velocity Layer (+ Cambrian)

Δz = 1.301 kms.

V = 2.83 kms/sec.

Mississippian Horizon

Δz = .839 kms

V = 5.12 kms/sec

Precambrian V = 6.00 kms/sec
(Assumed)

Fig. 13. Two Layer Surface Structure at Suffield as derived from Fig. 11.

Low Velocity Layer (+ Cambrian)

Δz = 1.264 kms.

V = 2.35 kms/sec.

Mississippian Horizon

Δz = .755 kms.

V = 5.32 kms/sec.

Precambrian V = 6.00 km/sec
(Assumed)

Fig. 14. Two Layer Surface Structure at Swift Current as derived from fig. 12.

basement surface was not good in either direction. Assuming that the velocity of P_g was 6.00 kms/sec, theoretical intercept times were calculated for this arrival at both shot points using the well velocity data. This theoretical time was then used when fitting the least squares line to the basement data. The assumed velocity is borne out further by the fact that the velocities obtained from the lines fitted to the experimental data are very close to the assumed figure of 6.00 kms/sec.

As is well known, much of Alberta and Saskatchewan is covered with a thin veneer of glacial material of one form or another. This was very evident along our refraction profile; we have not, however, made any correction for this surface low velocity layer. At most spread locations no information as to velocities and thickness of this layer are available, and it was further felt that such a correction would not enhance the data enough to warrant the expenditure in time.

3.2 Preparation of Travel Time Curves.

3.21 Timing

The time of the shot break was marked on the spread location records by one of several methods. As each truck was equipped with a chronometer, a WWV receiver and a standard broadcast receiver, the signal from each of these

was recorded on the seismic record. Before a days operation the shooting truck and the recording trucks decided which broadcast station would be recorded. Once on location, the chronometer was set from the WWV time signal, and if the signal was strong enough, the chronometer was rated by simultaneously recording the chronometer second marks with those of the WWV time signal. If, however, the signal was weak, then one had to rely on a different correlation device. Both the recording trucks and the shot point truck recorded the rectified, filtered output of the broadcast receiver set at the pre-arranged station. Then if one did not have the WWV time signal to correlate by, one could correlate the shot point and spread location records by using the broadcast station signal. In most cases it was possible to mark the shot break on all the records to within 2 or 3 milliseconds.

3.22 Distance Calculations

The geographic coordinates of both the shot point and each recording location (usually one read the coordinates of either the first or the last geophone in each location) were read off a large scale topographic map. An accuracy of ± .05 minutes can be expected from such a map. These data were then put on punch cards and the actual distance calculation was carried out on an IBM 1620 digital computer. The Department of Terrestrial Magnetism of the Carnegie Institute of Washington kindly lent the program to us. Hosmer's (1929) method was used in the program.

3.23 Spread Velocities

The phase velocities of each arrival in about the first five seconds after the first arrival were calculated for each record. This was accomplished by plotting the time interval between the trough or peak of an event on each trace against the geophone spacing. One then fitted a straight line through the points and calculated the mean velocity. An example of such a plot is shown in figure 15.

3.24 Travel Time Graphs

Once all these operations had been carried out, one could then begin to plot the travel-time curves. The type of plot used was the so-called reduced travel-time graph. This variety of plot was used because one could expand the time scale, thus enabling one to make more accurate correlations.

From each arrival time on a particular record was subtracted a time equal to the distance divided by 6.5. Hence, arrivals falling on a line whose slope would normally be the inverse of 6.5 would now fall on a line whose slope was zero. Each separate arrival on each record was plotted in its correct position in time and space on the travel-time curve. Then using both the records themselves and the travel time curves, lines were drawn through arrivals which were thought to come from the same refracting horizon. Once we were sure that we had indeed made the correct correlation, the line was fitted to its corresponding points in the least

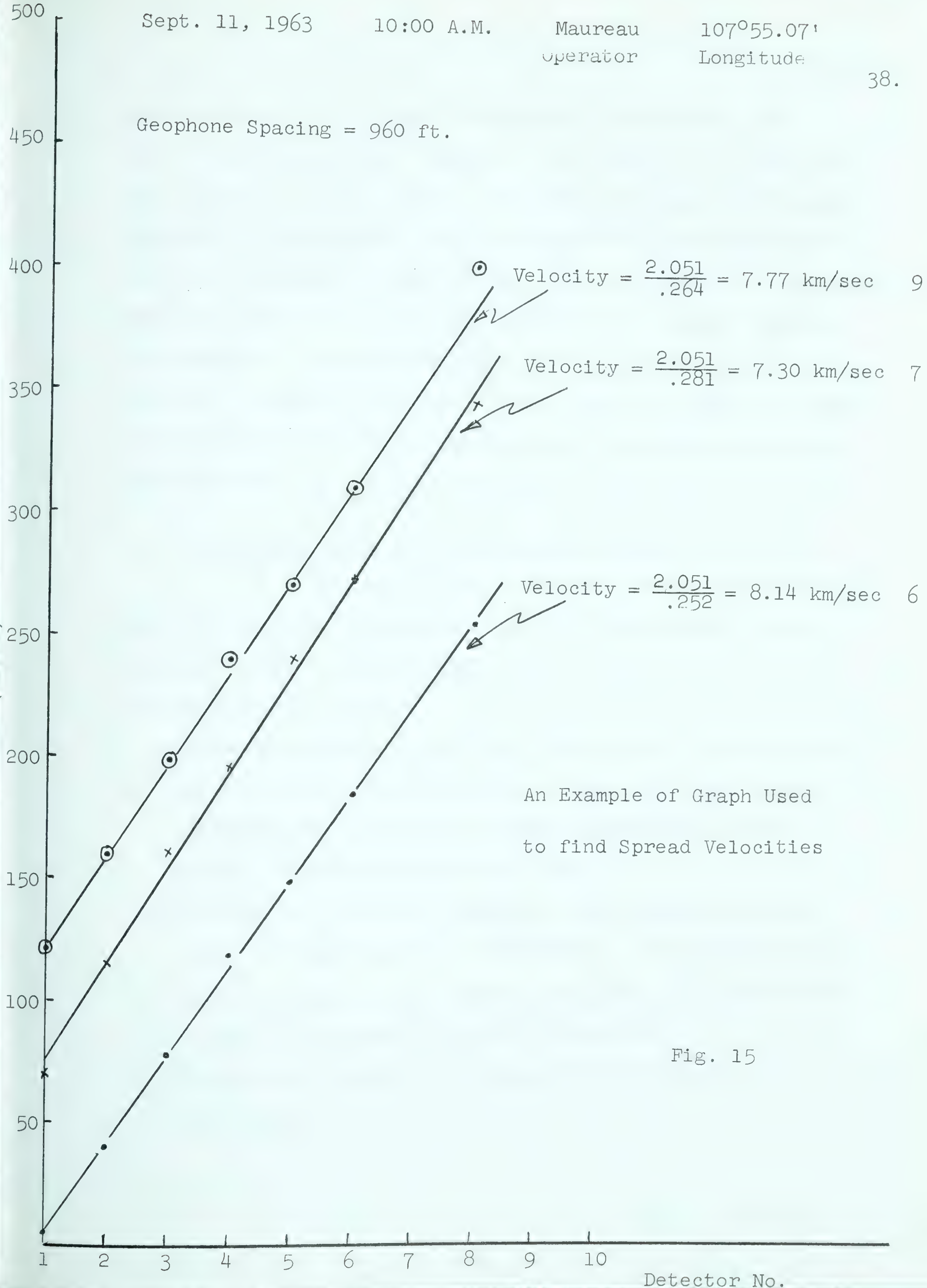

Sept. 11, 1963 10:00 A.M. Maureau 107°55.07' operator Longitude

Geophone Spacing = 960 ft.

Velocity = $\frac{2.051}{.264}$ = 7.77 km/sec 9

Velocity = $\frac{2.051}{.281}$ = 7.30 km/sec 7

Velocity = $\frac{2.051}{.252}$ = 8.14 km/sec 6

An Example of Graph Used to find Spread Velocities

Fig. 15

squares sense. From these statistical analyses we were able to deduce the zero distance time intercept of each line, the apparent velocity of the refracting horizon, the standard deviation of the slope, and furthermore, we could establish the 90 % confidence limits of the slope and the intercept times. Both of these latter two quantities are, of course, minimum uncertainties, since there are a number of other errors for which we can make no account. These types of errors include deviations in the refracting horizons from planar surfaces, miscorrelation of events, anisotropy in the horizon, etc.

3.3 Methods of Correlating Refracted Arrivals

P. S. Veitsman (1957) outlines the various criteria used to correlate various wave-groups from record to record on a continuous refraction profile. In essence, these criteria are as follows:

1. As one progresses further and further from the shot point, the refracted head wave which is the first arrival will correspond to a refraction from successively deeper seismic boundaries in the earth's crust.
2. The graph of the first arrival of each group of waves should be approximately rectilinear. Any departure from rectilinearity may be caused by relief on the refracting horizon or supraposed division boundaries.
3. The apparent velocity of successive waves in the same group should be similar.

4. The reverse times along a particular refraction line should be the same for any particular wave-group.

5. The apparent velocities of one wave group should be similar, whereas the apparent velocities of a different wave-group should be rather different.

6. There should be a relative maximum in amplitude in each wave group, provided that one is within the zone of interference: i.e., the zone where two different wave-groups interfere due to their similar arrival times.

7. There should be a determined regularity in the behaviour of the amplitudes on one wave-group from location to location, and furthermore, from profile to profile.

8. There should be an inherent stability in the form of the trace. That is, the waves of one group should have a similar appearance from record to record. We have found that this is particularly true of the Moho refraction, especially in the region close to the critical distance. For an example of this trait see Fig. 16.

9. Veitsman states that there should be a difference in the frequency of the arrivals from different horizons. He cites as examples from his work that the predominant frequency of the P* wave-group was from 9-10 cps, whereas the P_g wave-group had a dominant frequency range from 10-14 cps.

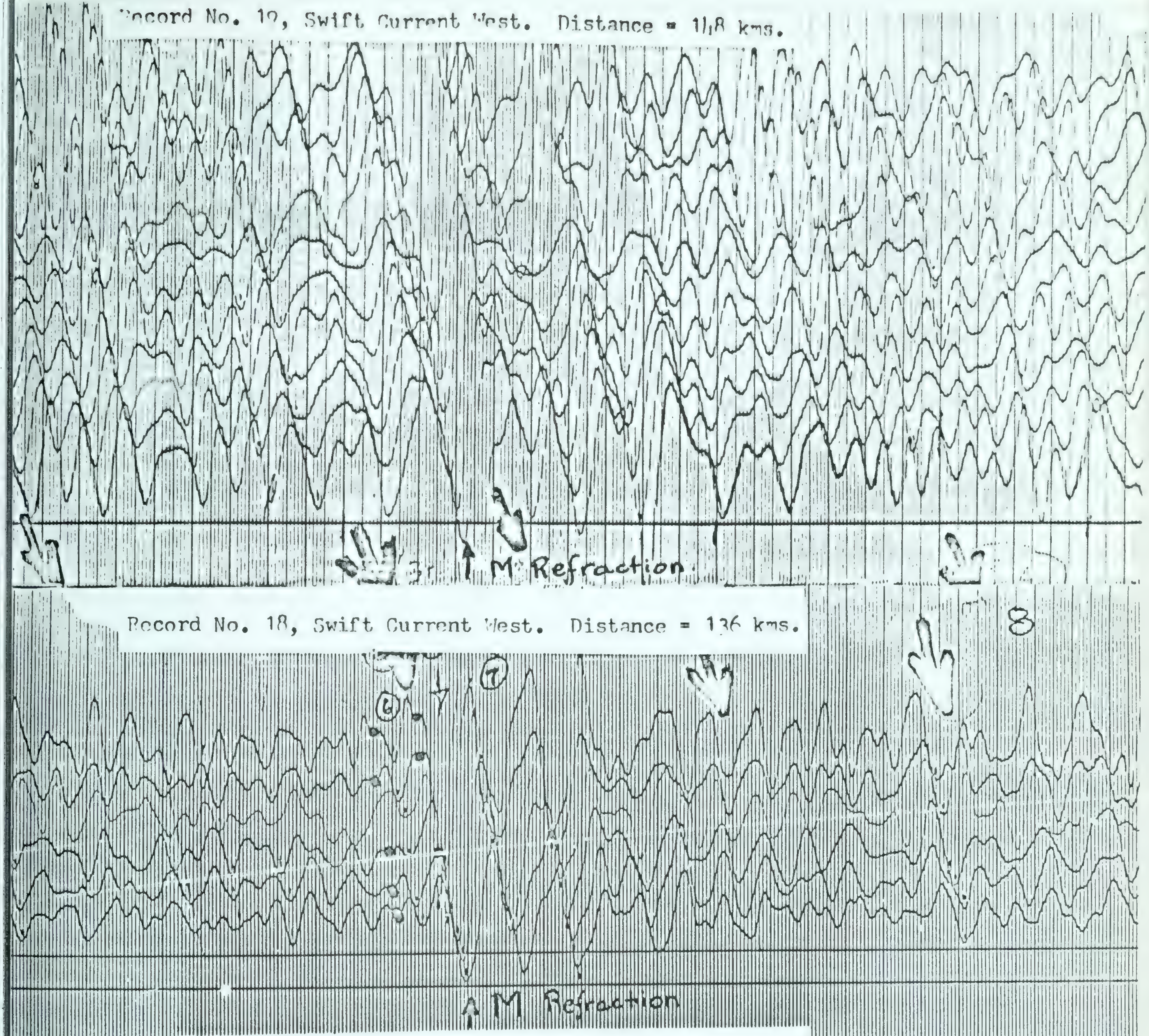

Record No. 19, Swift Current West. Distance = 148 kms.

Record No. 18, Swift Current West. Distance = 136 kms.

Fig. 16 Characteristic Near Critical Distance Moho Refraction

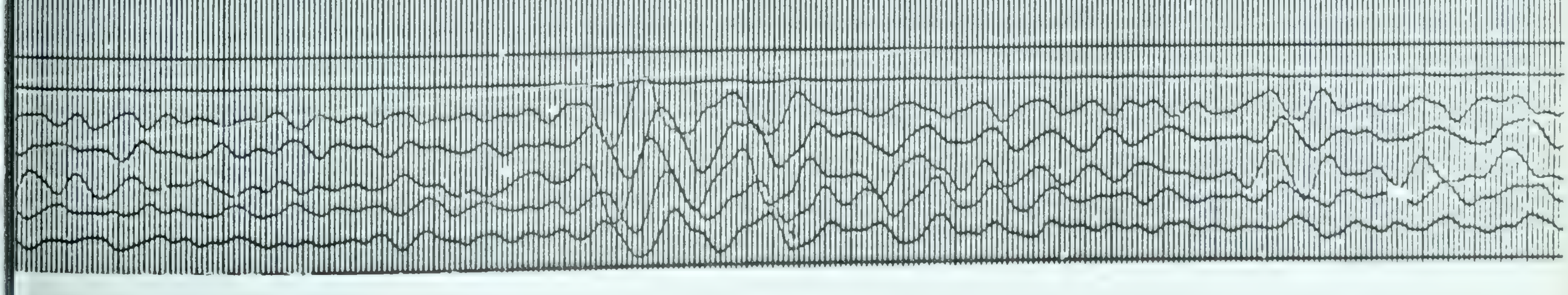

3.4 Discussion of the Travel-Time Graphs in the Light of these Criteria.

Figs. 18 and 19 illustrate the Suffield and Swift Current Travel Time Graphs respectively. During the last stages of correlation, the above criteria were used to a large extent in making the final choices. A number of problems arose, however, one or two of which have not really been resolved satisfactorily; rather we can only make an attempt to explain part of the problem away.

Criteria 1, 2, and 3 were satisfied on both travel-time curves. Criterion 4, however, is not satisfied. The reverse times between the Suffield and Swift Current shot points do not agree, the error being of the order of 400 milliseconds. Since there is so much data along the Swift Current line, we have decided to put all our faith into this interpretation, and lump all errors into the Suffield interpretation. In fact, we can show that this is not an unreasonable assumption.

We have seen that power spectral analyses of the Swift Current data indicate that the main bands of energy transmission are centred at about 5 and 10 cps, while similar analyses of the Suffield data indicate that the dominant frequency is about 5 cps. Let us assume that the velocity of propagation in the earth is not frequency dependent; hence the reverse times along a path should not depend critically on the frequency. This fact is probably true since the frequencies of interest are low.

Having established that there is a fundamental difference in frequencies along the reverse paths, we can account for at least part of the time delay. First, the shot holes at Suffield were drilled into a rather heavy boulder till, whose velocity of propagation is low. In addition to this, Jones (1963) points that there are a number of gravel lenses to be found in the general area of the shot point. Gravel beds are known to break up a wave-front rather badly, and have very low propagation velocities. Such an environment would certainly delay the wave front, although the magnitude of this delay time is indeterminate. A further consideration is that the resulting records from such a shot point have a very "loopy" appearance, there being little or no trace of character from record to record. Under such conditions correlation of events is very difficult, and the validity of interpretations made on such events is questionable. A further instrumental time delay is caused by the low frequency content of the signal. We should point out that the high - cut filter settings for most of the Suffield shots was 12 cps, while that of the Swift Current shots was 16 cps. There is a time delay of a few milliseconds due to this filter setting difference. Last, and perhaps most important, is the fact that the shot points and detector locations were not exactly reversed. Thus the reverse records

could not be tied exactly. Another factor which complicated the tying of events lay in the difference of the frequency content of the two records. There was no similarity between any of the events on the two records which should most nearly reverse time tie.

Criteria 5 and 6 were found to be true in general, but phase velocities of presumably similar events on the records from the Suffield line did not always match. This is considered to be a result of the "loopiness" of the records and ringing in the filter system, with a consequent running together of the various arrivals.

Criteria 7, 8, and 9 have been discussed previously.

Chapter 4

Here we shall present the final results of the calculations carried out to arrive at the proposed crustal model. The arguments both for and against will be presented, and the reasons for adopting the final model even in light of the argument against it. This model will be compared to that proposed by Weaver for the crustal structure west of Suffield. Finally, we shall present the results of the 500 ton trial at Suffield and give a tentative interpretation of the results.

4.1 The Layered Earth Model for Saskatchewan.

Using both continuous sonic velocity logs and the travel-time graphs derived from our experimental results, we have decided on a six layer earth model. These layers have been called the low velocity layer, the Mississippian horizon, the Precambrian basement, the sub-basement refractor, the Conrad discontinuity, and the Mohorovičić discontinuity. The final proposed model for the crustal structure in Southern Saskatchewan may be seen in fig. 17. Below is presented a set of tables which give all information regarding the various parameters used in the calculations. Where the errors are presented, these represent the 90% confidence limits.

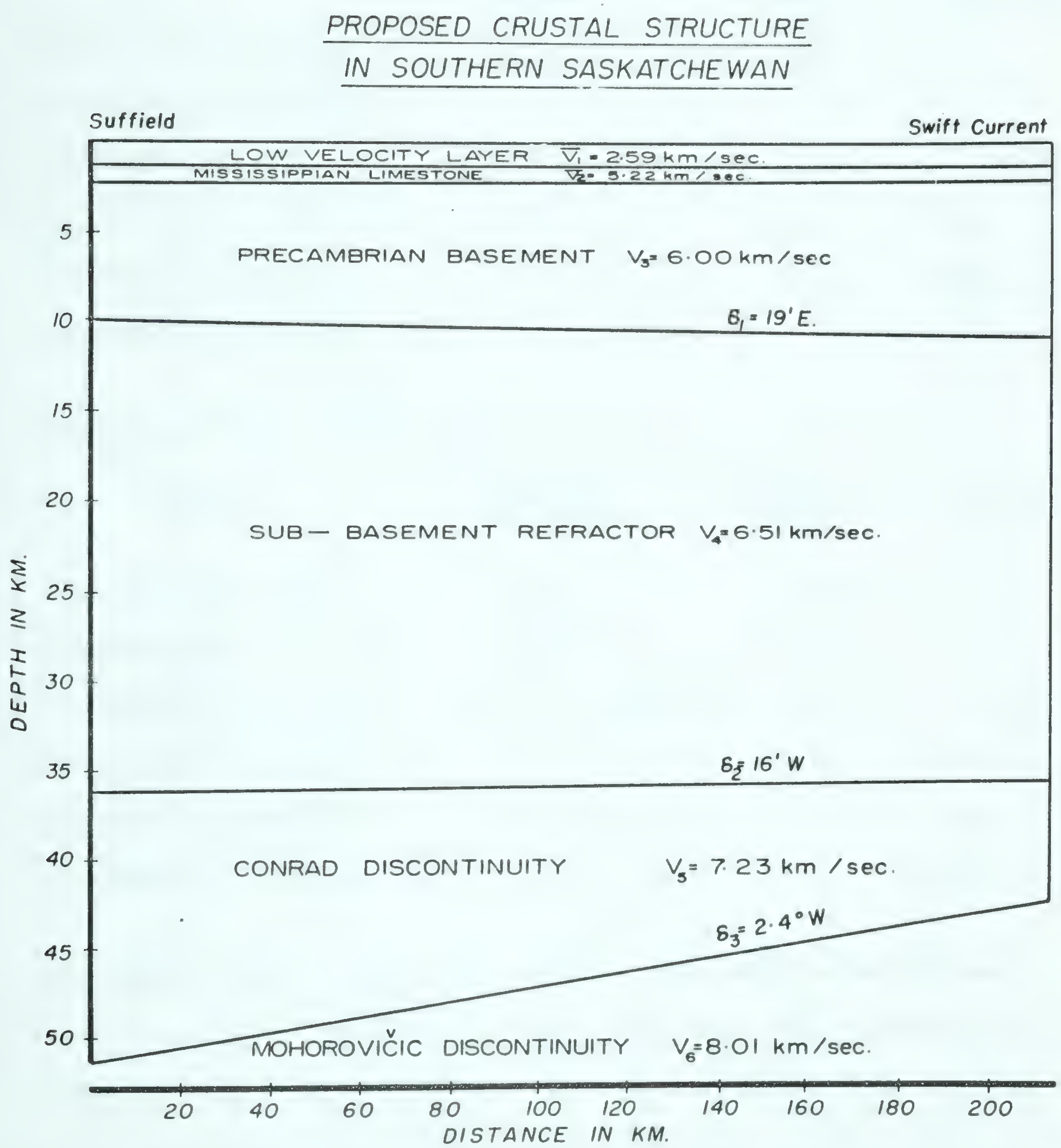
PROPOSED CRUSTAL STRUCTURE
IN SOUTHERN SASKATCHEWAN
Suffield
Swift Current
LOW VELOCITY LAYER $\overline{V}_1$ = 2·59 km/sec.
MISSISSIPPIAN LIMESTONE $\overline{V}_2$ = 5·22 km/sec.
PRECAMBRIAN BASEMENT V_3 = 6·00 km/sec
δ_1 = 19' E.
SUB— BASEMENT REFRACTOR V_4 = 6·51 km/sec.
δ_2 = 16' W
CONRAD DISCONTINUITY V_5 = 7·23 km/sec.
δ_3 = 2·4° W
MOHOROVIČIC DISCONTINUITY V_6 = 8·01 km/sec.
DEPTH IN KM.
5
10
15
20
25
30
35
40
45
50
20
40
60
80
100
120
140
160
180
200
DISTANCE IN KM.

Fig. 17

[illegible]

[illegible]

West Shot Point (Suffield)

Horizon	Velocity (kms/sec)	Thickness (kms)	Intercept Time (secs)
Low Velocity Layer	2.83*	1.30	
Mississippian Horizon	5.12*	.84	
Precambrian Basement	5.97+	7.77	.975'
Sub-basement Refractor	6.47 ± .04	26.15	2.031 ± .166
Conrad Discontinuity	7.21 ± .07	15.15	6.068 ± .263
Mohorovičić Discontinuity	8.06 ± .11		9.219 ± .416

East Shot Point (Swift Current)

Horizon	Velocity (kms/sec)	Thickness (kms)	Intercept Time (secs)
Low Velocity Layer	2.35*	1.26	
Mississippian Horizon	5.32*	.76	
Precambrian Basement	6.00 (assumed)	8.87	1.121'
Sub-basement refractor	6.55 ± .10+	24.61	2.307 ± .125
Conrad Discontinuity	7.25 ± .01	6.86	6.093 ± .060
Mohorovičić Discontinuity	7.99 ± .05		8.422 ± .147

The travel-time curves from which these data were derived may be seen in figs. 18 and 19. The other two parameters of interest in the final model are the true velocities of the

---

* These velocities are calculated from the continuous sonic velocity logs

\+ These velocities, and the velocities below this refractor represent apparent velocities.

' This is a theoretical intercept time calculated from well log data.

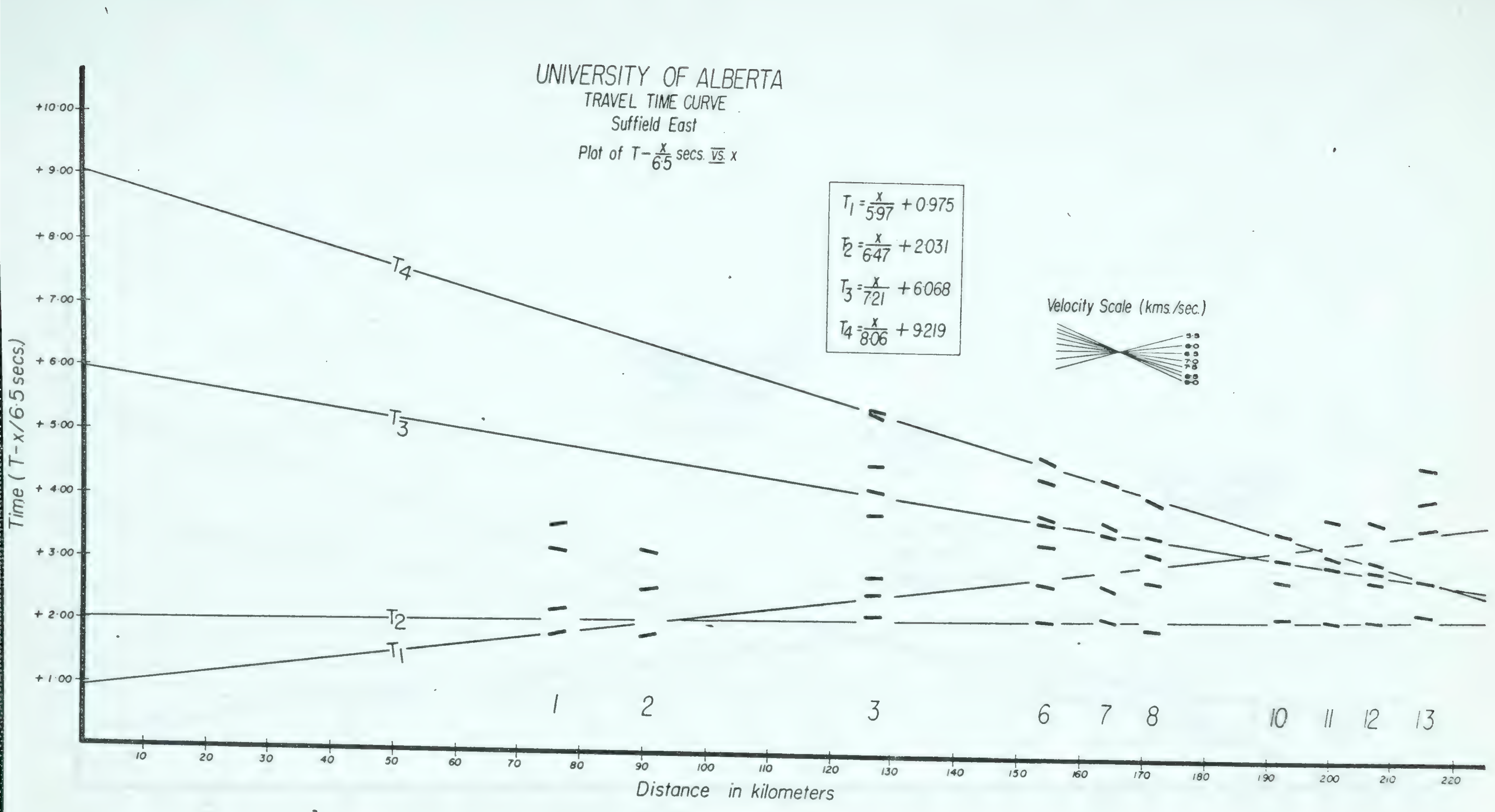
UNIVERSITY OF ALBERTA
TRAVEL TIME CURVE
Suffield East
Plot of $T - \frac{x}{6\cdot5}$ secs. $\underline{VS.}$ x
$T_1 = \frac{x}{5\cdot97} + 0\cdot975$
$T_2 = \frac{x}{6\cdot47} + 2\cdot031$
$T_3 = \frac{x}{7\cdot21} + 6\cdot068$
$T_4 = \frac{x}{8\cdot06} + 9\cdot219$
Velocity Scale (kms./sec.)
5·5
6·0
6·5
7·0
7·5
T_4
T_3
T_2
T_1
1
2
3
6
7
8
10
11
12
13
Time (T-x/6·5 secs.)
+10·00
+ 9·00
+ 8·00
+ 7·00
+ 6·00
+ 5·00
+ 4·00
+ 3·00
+ 2·00
+ 1·00
10
20
30
40
50
60
70
80
90
100
110
120
130
140
150
160
170
180
190
200
210
220
Distance in kilometers

Fig. 18

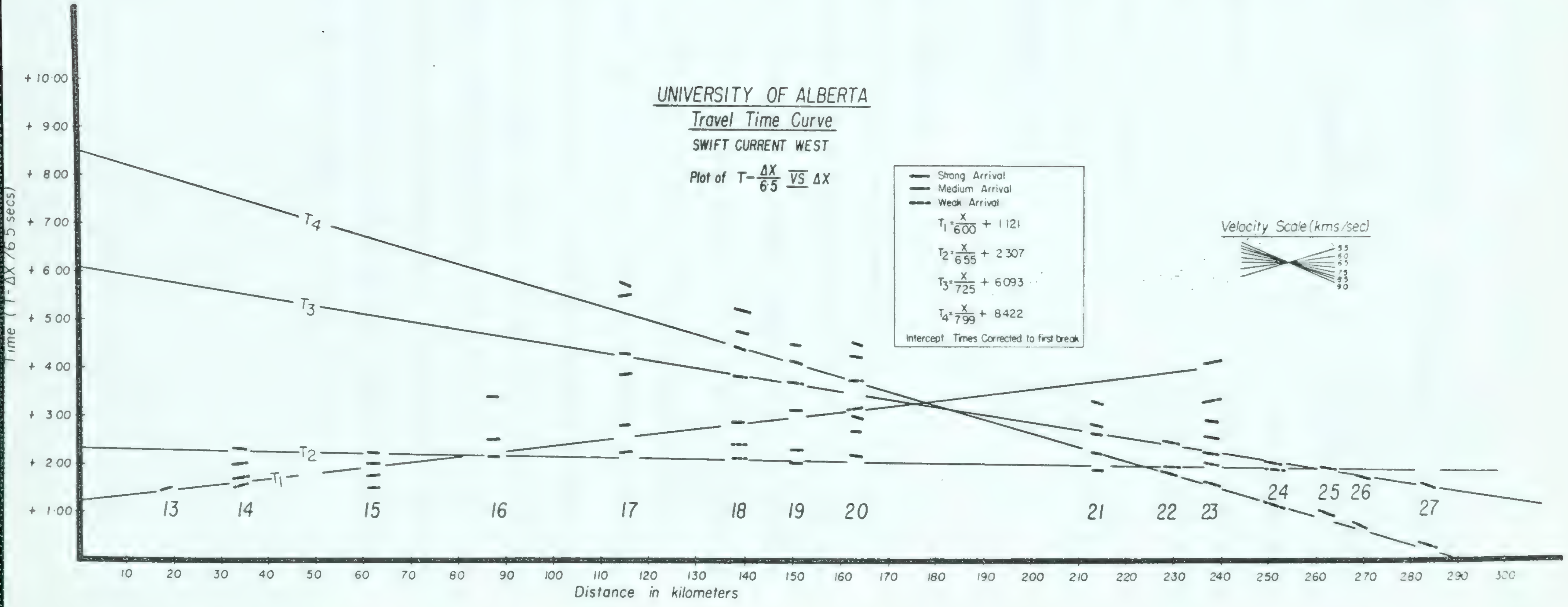
UNIVERSITY OF ALBERTA
Travel Time Curve
SWIFT CURRENT WEST
Plot of $T-\frac{\Delta X}{6.5}$ VS ΔX
Strong Arrival
Medium Arrival
Weak Arrival
$T_1=\frac{X}{6.00}+1.121$
$T_2=\frac{X}{6.55}+2.307$
$T_3=\frac{X}{7.25}+6.093$
$T_4=\frac{X}{7.99}+8.422$
Intercept Times Corrected to first break
Velocity Scale (kms/sec)
5.5
6.0
6.5
7.5
8.5
9.0
T_1
T_2
T_3
T_4
13
14
15
16
17
18
19
20
21
22
23
24
25
26
27
Time ($T-\Delta X/6.5$ secs)
+ 1.00
+ 2.00
+ 3.00
+ 4.00
+ 5.00
+ 6.00
+ 7.00
+ 8.00
+ 9.00
+ 10.00
10
20
30
40
50
60
70
80
90
100
110
120
130
140
150
160
170
180
190
200
210
220
230
240
250
260
270
280
290
300
Distance in kilometers

Fig. 19

layers and the dip of the layers. They are as follows:

Horizon	Dip (degrees)	True Velocity (kms/sec)
Low Velocity Layer	0	2.59 (average)
Mississippian Limestone	0	5.22 (average)
Precambrian Basement	0	6.00 (assumed)
Sub-basement Refractor	19' E	6.51
Conrad Discontinuity	16' W	7.23
Mohorovičić Discontinuity	2.4 W	8.01

4.2 The Travel-Time Graphs.

The travel-time curves shown in figs. 18 and 19 represent the data from the Suffield and Swift Current shot points respectively. Some 10 records were used to compile the Suffield travel-time graph, while 15 records were used to compile the Swift Current graph. These curves were discussed earlier, but we must now discuss them in terms of the proposed crustal structure. In both cases we note that the intercept times have been corrected to the first break, the correlations having been made in the first trough. Arrival amplitudes have been graded for the Swift Current data, but not for the Suffield data, since the latter are not considered to be as reliable.

.1 Suffield Shot Point.

The only horizon for which good first arrival control exists on the Suffield curves is the sub-basement refractor. There is little doubt as to the validity of this correlation. The basement refractor has been constrained to fit a theoretical intercept time calculated from well logs; the number of points used to fit this line are minimal. Correlation of the Conrad and Moho events is not considered to be very reliable in the light of the low frequency character of the records. This is also evident in the statistical errors calculated for the slope and intercept time parameters. The error in the intercept times is especially high for both these events; in fact, it is high enough to account for the non-reverse time tie. Spread velocities are not everywhere consistent with the calculated apparent velocities. This is especially evident on the sub-basement refractor line and the Moho correlations. Such discrepancies tend to further reduce the reliability of the data. We should keep in mind, however, the low frequency character of the data and the sharp band-pass of the filters used for most of the recordings. Both of these facts would tend to give erroneous spread velocities since the events are not clearly separated from one another, with consequent interference taking place. Although we cannot

claim interference for the first arrival, we do note that a high spread velocity is sometimes consistent for all arrivals throughout the record, while on other records this is not the case. No good explanation is available for this phenomenon.

4.22 Swift Current Shot Point.

The Swift Current travel time graph, on the other hand, is much more reliable in many respects. We see from fig. 19 that the first arrival control for two out of the four refractors is very good (the sub-basement and Moho), while control for the basement refraction is much better than that at Suffield. Once again the basement data have been constrained to pass through a theoretical intercept time. It is evident on the travel-time curve that more than one correlation is possible for the basement event. We have chosen the final correlation for the following reasons. First, the apparent velocities of the arrivals used for this correlation were quite consistent with the assumed basement velocity. Secondly, the close-in refraction work (records 13 and 15) was done subsequent to the original pick, and the data from these two records indicated that the final pick was more reasonable. There is certainly no doubt about the sub-basement and Moho arrival correlations, since in both cases correlation by character was possible;

spread velocities agree very closely with the apparent velocity calculated; and first arrival control was very good. In order to illustrate the definitive nature of correlation by character we can consider the M arrivals picked on records 18 and 19. These arrivals were very strong, and had a character which is considered to be diagnostic of this arrival (see fig. 16). Correlation of the events on records 21 and 23 with the former events gave a good line, whose velocity was close to that defined for the Moho. Subsequent refraction work (records 22, 24, 25, 26 and 27) gave good first arrival control on the M refraction, and a line drawn through these events tied almost exactly into the line drawn on the basis of second arrival information. Furthermore, the statistical analyses tend to bear out the correlations we have made. The Conrad event is felt to be quite well defined. Statistical calculations made, substantiate the rectilinear nature of the correlations, and the time intercept error is especially low. There is always a certain amount of doubt in using second arrival information, but the doubt in this case is considered minimal. Having discussed the travel time curves as separate entities divorced from the crustal structure, let us now consider the two curves in conjunction with the proposed model seen in fig. 17.

4.3 Pros and Cons of the Proposed Crustal Structure.

4.31 Cons.

There are two serious objections to the proposed crustal structure. These are the non-reversing time tie, and the fact that the apparent velocities for the M refraction are not consistent with the dip shown in fig. 17. The dip shown is not calculated using the usual equations, but is simply the dip as defined by the depths under each shot point.

The non-reversing time was discussed previously. Although we could not account for it fully, we could at least explain part of the discrepancy. We further note that the errors in the intercept times for the various arrivals at Suffield data are almost high enough to cover the 400 milliseconds error in the time tie. We feel that this is not a very serious objection in light of the poor data along the Suffield line.

The fact that the apparent velocities are very nearly equal is a more serious objection, this condition implying little or no dip. The velocity under Swift Current (7.99 kms/sec) is consistent, while the velocity under Suffield (8.06 kms/sec) is too low to account for the dip indicated by the intercept times. The errors nearly cover this uncertainty, although this does not afford the best explanation. An alternative explanation is

available. If we assume that the dip becomes shallower under Suffield, then we can easily account for the close apparent velocities. Weaver's model does, in fact, suggest that the dip under Suffield is much less than that which we have indicated in fig. 17. If this is indeed the case, then we need not worry about the discrepancy in the velocities, since this latter modification would justify the observed values.

The final objection to the model lies in the lack of coherency between the model proposed by Weaver (1962) for the structure between Suffield and Vulcan, and that proposed by us. In essence, the two models are similar in that they both are six layer models, and the crustal thicknesses calculated are quite compatible. We do not postulate a low velocity layer as Weaver has done since we have no data to indicate that such a layer exists in Saskatchewan. Although Weaver substantiates his argument for such a layer very well, we see no reason to include it in our model. The reasons are that we have no discrepancy between the theoretical critical distance for the M arrival and the observed critical distance, and furthermore, the Bouguer gravity anomaly suggests that the low velocity layer pinches out just east of Suffield. There is some suggestion of this layer observed on the Swift Current travel-time curve. The last three Moho refractions appear to come in just a little late suggesting a delay for these locations caused by a low velocity horizon (Fig. 19).

4.32 Pros.

There are several facts which we feel substantiate our model, and most important, override the arguments against it. Let us first consider the Suffield data. Although we have already pointed out the many discrepancies, the intercept times calculated for the Moho and Conrad events agree closely with those calculated by Weaver (1962). Secondly, from the extension of the Suffield west data into the mountains this last summer, the intercept time calculated for M at Suffield was about 9.25 seconds; again agreeing very closely with what we have calculated. This is an indication that the picks made are not completely miscorrelated events.

Certainly the excellent first arrival data shown in the Swift Current curves substantiates the structure under that shot point. The excellence of the statistics further bears witness to the reliability of this profile.

Even though this model represents a straightforward interpretation of the data, it fits extremely well with the observed data. The Moho critical distance calculated for it is very close to that observed on the records. We have calculated a critical distance of 132 kms. for the model. The observed critical distance (as judged by the location of the first strong arrivals from M) on the graphs is about 125 kms. for the Suffield profile, and about 135 kms. for the Swift Current profile. This is a remarkably good fit, and helps to strengthen our interpretation.

4.4 Comparisons with other data

1) McCamy and Meyer (1964) have shown a number of crustal profiles completed in Montana, just south of our own line (see fig. 20). The most important of the profiles is in Eastern Montana. The model they obtain for the crust is similar in all respects to that postulated by us. Although the near surface structure is one layer of 2.8 kms/sec, there are four other layers which correspond to our Precambrian basement, the sub-basement refractor, the Conrad discontinuity and the Mohorovičić discontinuity. The velocities for each of these horizons are 6.1, 6.4, 7.8 and 8.3 kms/sec respectively. The dips shown in their diagram correspond in general with those found by us. That such close correlation should exist between two profiles done completely independently is a good indication that the model for Saskatchewan is generally correct.

2) Weaver (1962) discusses the work done by Richards and Walker (1959), and has replotted the data used by them; arriving at a new interpretation using rather different results. His final model suggests that the sub-crustal velocity is about 8.2 kms/sec and the Conrad velocity is about 7.2 kms/sec, the crustal thickness being about 43 kms and the depth to the Conrad being about 26 kms. The interpretation used by Richards and Walker suggest the same velocities but the depth to the Conrad was 29 kms (as opposed to 26 kms) and the crustal thickness is about 43 kms (the same as Weaver

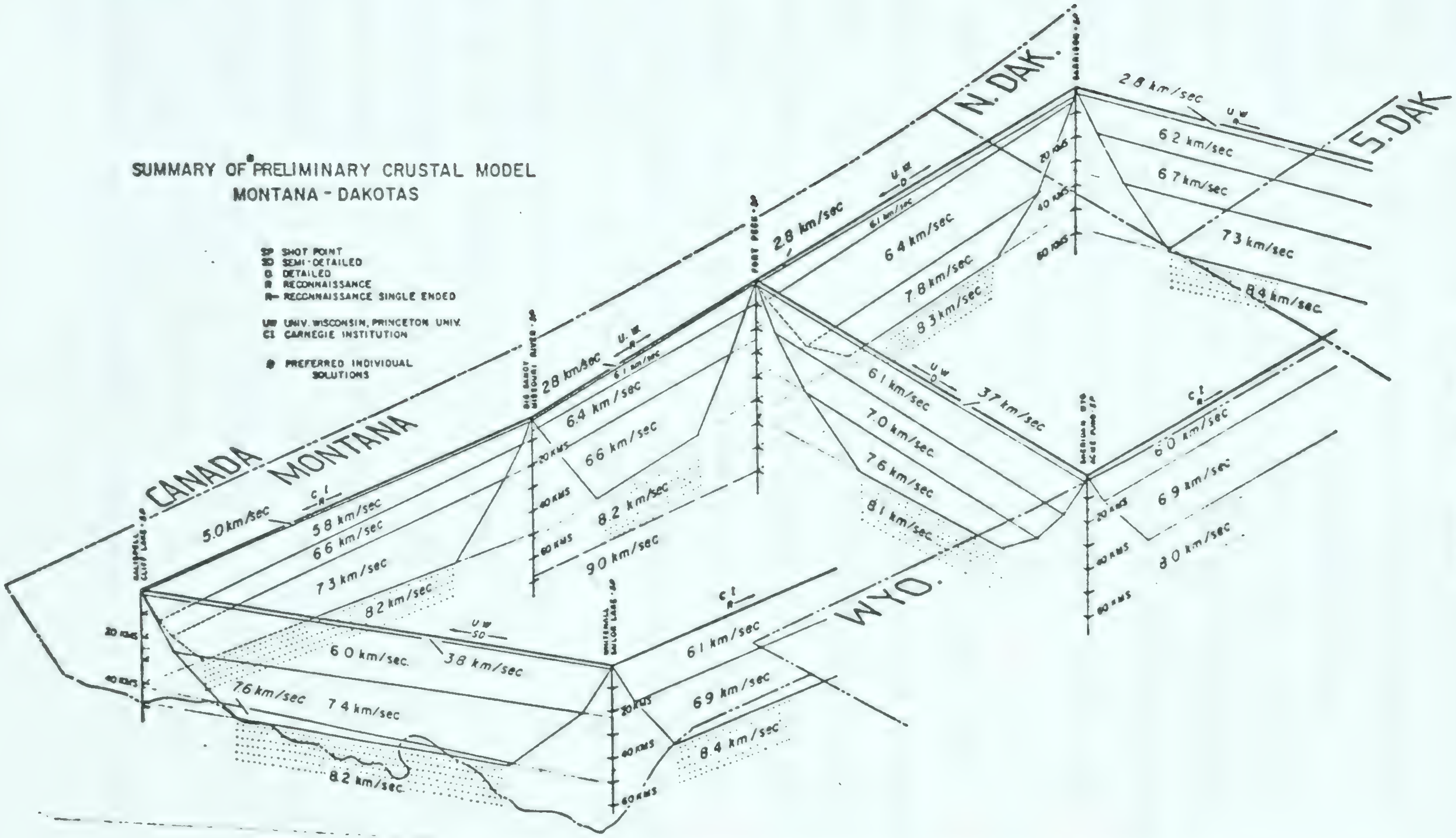

Fig. 20 Summary of preliminary crustal models in Montana-Dakota region. All profiles are interpreted independently.

obtained). The models obtained by Weaver and by Richards and Walker are not at all at odds with each other, in fact, their relative closeness would suggest that although the authors are not in agreement with each other, their separate interpretations are not invalid. The present author has not recalculated the work done by Richards and Walker, but rather wishes only to point out that the depths to the various horizons postulated by them are shallower than those given by both Weaver and ourselves. A very short profile was shot (only 132 kms.), and scanty data were obtained from the records. The interpretation was based on second arrival information for the Conrad and Mohorovičić discontinuities, which at the best of times is not nearly so good as using first arrival information. Furthermore, interpretation of seismic data is often subject to personal biases on the part of the seismologist, this being a bias which is hard to account for. Reinterpretation of data is naturally going to be subject to a different bias and the resulting interpretation cannot be expected to be exactly the same as the original. Perhaps a more accurate picture would be a composite of the two. We do not feel that the Richards and Walker profile is completely in error, rather we feel that the profile is too short to allow a very detailed description of the crustal structure in the area.

Although the crust proposed by them is thinner than the plains structure, it is in line with data recently obtained by ourselves in the profile shot from Suffield west into the Rocky Mountains. These data suggest that the crust thins under the foothills, the velocity being about 8.2 kms/sec. A remarkably close correlation thus exists between the data obtained by Richards and Walker and our own data, even though the Rocky Mountain data cannot be subject to a definitive interpretation (see 4.5).

3) Recently Hall and Brisbin (1961) completed a single ended refraction profile near the Flin Flon area in Manitoba. The principal results obtained from this survey are:

a. A three layer earth was postulated:

depth to the Conrad discontinuity = 16.5 ± 1.1 kms
depth to the Moho discontinuity = 35.2 ± 1.4 kms

These values are markedly different from those obtained by us. We should, however, point out that the seismic-refraction survey was carried out along or near the boundary between the Churchill and Superior geologic provinces. Since these two provinces show such different ages, it is not unreasonable to assume that there might be quite different conditions existing for the deep crustal layers. The Moho dip calculated for the Saskatchewan data is such that if it is extrapolated

into Manitoba, the crustal thickness would compare favorably with that described above. The Conrad in Saskatchewan shows remarkably little dip, and is not at all compatible with that described by Hall and Brisbin. The fact that the Manitoba profile was shot near the boundary of the two provinces is felt to influence this horizon to some extent.

b. Their velocities are as follows:

$P_g = 6.15 \pm 0.05$ kms/sec

$P^* = 7.10 \pm 0.05$ kms/sec

$P_n = 8.17 \pm 0.06$ kms/sec

These velocities are well within the range of the accepted parameters, and agree quite closely with those obtained by ourselves.

4) Evidence for intrabasement discontinuities is found in many areas. Robertson (1963) has found reflections from an intrabasement layer in Southern Alberta, in an area south of Weaver's line. Work by Junger (1951) in Big Horn County, Montana and by Widess and Taylor (1959) near the Wichita Mountains of Oklahoma has indicated that intrabasement layers exist in other areas. A similar discontinuity in our own area might be the source of our 6.5 km/sec arrival. In light of the complicated nature of the Precambrian basement, the existence of such layers should not be too surprising. They might represent the roof of a batholith or some other large intrusion, or they might represent the boundary between different geologic provinces.

We do not have enough data to substantiate any of these hypotheses.

As a consequence of the foregoing remarks, we feel that the model postulated for the earth's crust in southern Saskatchewan is a reasonable model. The agreement of the theoretical model with the experimental data is remarkably good. The fact that an independent refraction profile shot in Montana, just south of our line, agrees in general form with our own is further justification for our model. The statistical analyses of our data are certainly good for the Swift Current line, and the layered structure at this shot point is believed to be correct. The agreement of crustal thickness at Suffield between our own model and that of Weaver for the western plains is also very good. All these facts increase our confidence in the proposed structure.

4.5 Suffield 500 Ton Trial and the Rocky Mountain Data

In July of 1964, the Defence Research Board of Canada, at the Suffield Experimental Station, detonated 500 tons of TNT on the surface of the ground. Ten seismic records were obtained from this shot, ranging in distance from 200 kms to 500 kms. from the shot point. Eight of these records were provided through the courtesy of the U. S. G. S. Crustal Studies Group seismic crews, one was supplied by Dr. Hugh White of the Dominion Astrophysical

Observatory, Victoria, British Columbia, and one record was provided by ourselves. These results were compiled and plotted on a reduced travel-time curve (fig. 21).

This diagram illustrates first the surface topography, and below, the reduced travel-time data. The reduction factor is X/8.25. This reduction factor was chosen since Weaver obtained a velocity of 8.25 kms/sec for the Moho under the plains. The squares and the triangles represent the reversed travel-time data used by Weaver, the intercept time of this data being about 9.2 secs. This time corresponds to a depth of about 46 kms. The circles represent the new extension of the lines, also reduced at 8.25 kms/sec. As one readily observes, there is a definite structural implication in the reduced times. We must, however, point out that these data are in the raw state, since no correction has been applied to account for elevation or for the high speed overburden which exists in the mountains. The effects of these factors are discussed below. Since no reverse profile was shot, a definitive interpretation is not possible; as a consequence, we shall present several alternative interpretations.

All the points have been displaced to the point of their approximate emergence from the Moho; thus any structure in the time domain is in its correct location with respect to

REDUCED TRAVEL-TIME GRAPH OF DATA
FROM SUFFIELD WEST

(Points displaced to place of emergence from MOHO.)

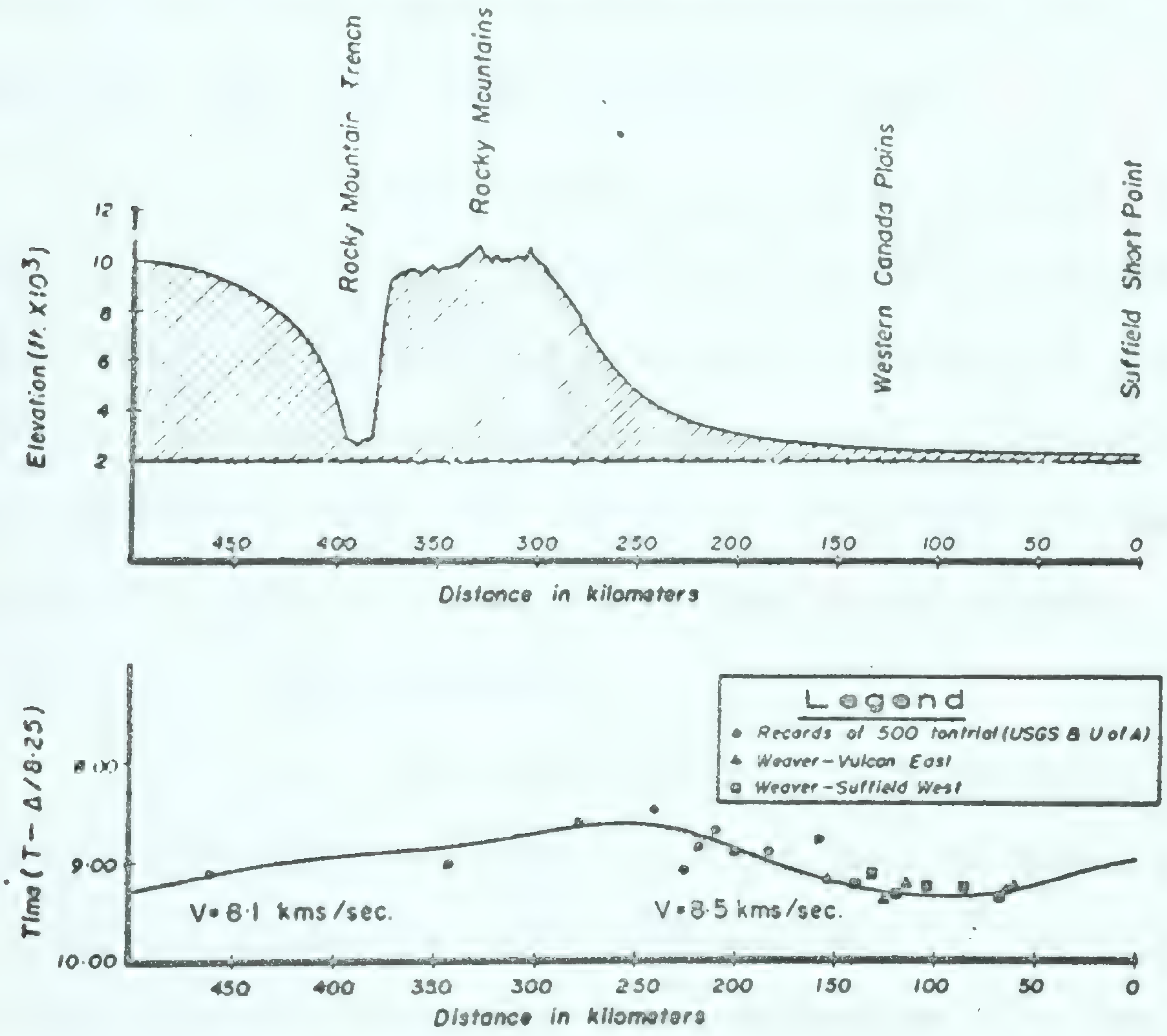

Fig. 21

[illegible]

[illegible]

the surface topography. The first interpretation is the following. Let us assume that the depth of the Moho remains constant under the mountains (this would be about 46 kms as derived by Weaver). The changes in slope indicated on the travel-time graph then imply that there is a velocity gradient from east to west starting under the foothills. The change in slope is equivalent to a velocity of 8.5 kms/sec under the foothills (see fig. 21) breaking to a velocity of 8.1 kms/sec under the Rocky Mountains proper.

The next interpretation is one in which it is assumed that the time variations are due to structural changes under the mountains, and not to changes in the velocity of the Moho. In this case, the Moho appears to become shallower under the foothills, the order of magnitude being about 5 kms, and then thickening again slowly to the west under the Rocky Mountains.

The final, and most probable interpretation, is a combination of the above two. In this case we would postulate a velocity gradient from 8.25 kms/sec in the plains to about 8.00 kms/sec under the Rocky Mountains. In the light of this velocity variation, there would be a thinning of the crust under the foothills, and then a roughly constant thickness under the mountains, the depth to the Moho being about 35-40 kms. This latter interpretation is in good agreement with that postulated for the Southern Rocky

Mountains (Mr. L. C. Pakiser, personal communication), the velocity gradient being in agreement with results published by Stuart, Roller et al (1964).

We prefer this latter interpretation, but a final answer is dependent on the measurement of the true velocity of the Mohorovičić discontinuity by means of a properly reversed profile in the mountains. Below we present a few speculations regarding isostatic compensation and a discussion of the effect of the overburden on the observed intercept times.

4.51 The Effect of Overburden.

Calculations made to correct for elevation and overburden in the Rocky Mountains indicated that the correction to the data is negligible. At most, the arrivals are some 0.10 seconds too early with respect to the arrivals in the plains. The following is a list of the residual time to be added to the intercept time to correct it to the approximate level of the plains:

From west to east the time residual (in seconds) per record is

.10
.16
.00
.03
.03
.10
.10

By observing the curve shown in fig. 21 we see that these values do not change the shape of the curve, only lower its west end by a factor of about .10 seconds in time. This only implies that the depth to the Moho is changed by about 1 km at most (i.e., the Moho becomes 1 km deeper). Our final conclusions regarding the structure still stand.

4.52 Isostatic Compensation.

Although the data are unreversed, and not really corrected for any sort of crustal variations, they do suggest that the crust is thinning under the mountains. We felt that it would be instructive to look at the two theories of isostasy, and do some calculations upon the data. The two most widely quoted theories of isostasy are the Pratt-Hayford Isostatic System and the Airy-Heiskanen Isostatic System. The assumptions of the Pratt-Hayford System are as follows:

1. Isostatic Compensation is uniform; i.e., the density underneath mountains is uniformly less than under flat land.
2. The compensating layer is located directly underneath the mountains and reaches to the depth of compensation D, where equilibrium prevails.
3. The density p' of the compensation, corresponding to a topographic elevation h, and the density p of the topography satisfy the equation

$$p' = - \frac{h}{D} p$$

4. The depth of compensation is everywhere equal when measured from the physical surface of the earth and not from sea level.

The assumptions of the Airy-Heiskanen system can be summarized as follows:

1. Isostatic compensation is complete.
2. The compensating layers are directly under the topography.
3. The density of the earth's crust is everywhere 2.67.
4. The density of the underlayer is also constant everywhere, having a density which is 0.6 higher than the density of the crust.

These assumptions imply a root of crustal material under the mountains.

From our data it is apparent that the Pratt-Hayford theory of isostasy is more applicable. Considering this as our isostatic model, we calculated the depth of compensation for the Rocky Mountains using several different models to demonstrate how this depth varies with varying parameters. We have, of course, assumed that isostatic equilibrium prevails in the mountains, but this is approximately true (see Heiskanen and Vening Meinesz, 1958, Garland and Tanner, 1957).

Below we present some of the various models we have used to calculate the depth of compensation. The following parameters were varied in the calculations: the density of the crustal material, the density of the mantle material, and the average height of the Rocky Mountains. The densities were deduced from curves published by Nafe and Drake (1954?). Fig. 22 is the schematic model used to calculate the level of compensation.

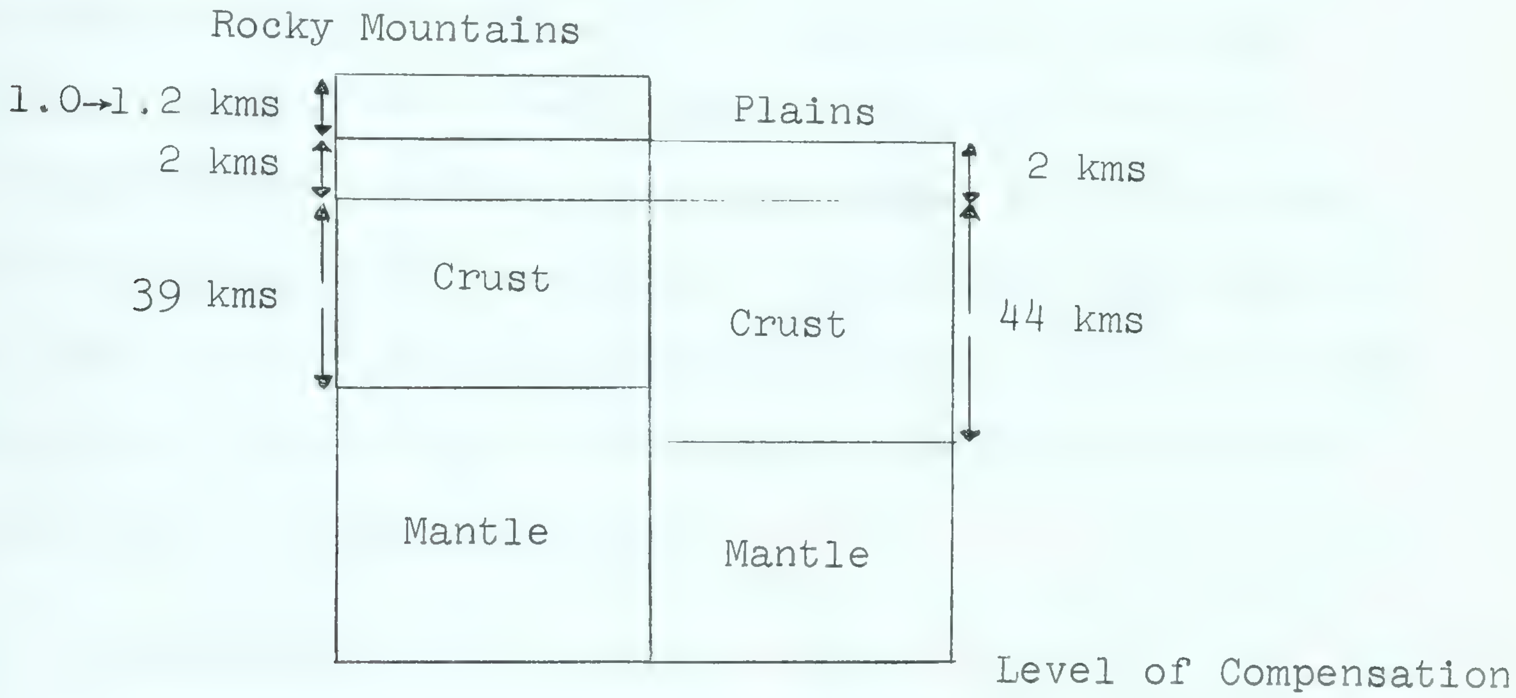

Fig. 22

The following parameters were kept constant throughout the calculations. The thickness of post Precambrian materials under the plains was 2 kms, and the density was 2.67. The thickness of the crust under the plains was 45 kms, and the thickness of the crust under the mountains was 40 kms (not including the sedimentary section).

Reference to Table 2 gives the various models calculated. We see that the average sort of model has a depth of compensation of about 116 kms to 118 kms. We further note that this level of compensation is rather insensitive to variations in crustal velocities and variations in the average height of the mountains. They are, however, very sensitive to changes in the mantle velocity. The change under the mountains of 8.00 to 7.80 kms/sec produces a change in the level of compensation of some 35 kms. The numbers we have derived for the level of compensation of the Rocky Mountains bear a startling similarity to the level of isostatic compensation that Hayford and Bowie calculated for the United States, namely 113.7 kms. Whether our numbers are coincidental or whether they are significant remains to be seen.

4.6 Conclusions

From all the calculations made, we have derived a six layer earth model for southern Saskatchewan. These layers we have called the Low Velocity Layer, the Mississippian Layer, the Precambrian Basement, the Sub-basement refractor, the Conrad discontinuity, and the Mohorovičič discontinuity. The velocities calculated for these layers are

V_1 = 2.59 kms/sec

V_2 = 5.22 kms/sec

V_3 = 6.00 kms/sec (assumed)

V_4 = 6.51 kms/sec

V_5 = 7.23 kms/sec

V_6 = 8.01 kms/sec

Model No.	Average Thickness of Mountains (kms)	Density of Crust	Density of Mantle under Mountains	Density of Mantle under Plains	Level of Isostatic Compensation
1	1	2.86 (≡ V = 6.4 km/sec)	3.38 (≡ V = 8.00 km/sec)	3.46 (≡ V = 8.25 km/sec)	118 kms
2	1	2.89 (≡ V = 6.5 km/sec)	3.38	3.46	116 kms
3	1	2.92 (≡ V = 6.6 km/sec)	3.38	3.46	114 kms
4	1	2.89	3.33 (≡ V = 7.8 km/sec)	3.46	87 kms
5	1.1	2.89	3.38	3.46	120 kms
6	1.2	2.89	3.38	3.46	122 kms

Table 2

The depths under the shot points of each of the layers are as follows:

Under West Shot Point		Under East Shot Point	
Mississippian	= 1.30 kms	Mississippian	= 1.26 kms
Precambrian	= 2.14 kms	Precambrian	= 2.02 kms
Sub-basement	= 9.91 kms	Sub-basement	=10.89 kms
Conrad	=36.06 kms	Conrad	=35.50 kms
Moho	=51.21 kms	Moho	=42.36 kms

The dips for each of the layers may be observed in fig. 17.

Although this model does not agree with that postulated by Weaver for the crust just west of Suffield, there are many features of our model which suggest that the true structure to the west is not the same as that which we have found. First, the Bouger anomaly which Weaver uses as part of his proof dies out just east of Suffield. Secondly, we have calculated the critical distance for the Moho refraction and find that it agrees very closely with that observed on the records (about 130 kms). Thirdly, the crustal structure which we have postulated agrees very well with the crustal structure in Montana, along a line parallel to our own, but south of us (see McCamy and Meyer as well as fig. 20). Although the Conrad does not dip very much, the Moho dips some 2 degrees to the west, and the

implication is that eventually the Conrad will pinch out to the east. This agrees with present data in eastern Canada although the Lake Superior Experiment may reveal this layer (Mr. Malcolm Bancroft, personal communication). The sub-basement refractor which we have found is not unreasonable since other people have reported seeing reflections from intra-basement layers. On the whole, we feel that the model which we have postulated is a very realistic model.

The extension of the Suffield data to the west has produced some interesting results. Until either converted phases are analyzed, or a reverse profile is shot, a definitive interpretation is not possible. Some alternatives have been presented. The most reasonable interpretation seems to indicate that there is a west-east velocity gradient of about 8.25 kms/sec under the plains to about 8.00 kms/sec under the foothills. In addition, it appears that the crust thins from 46 kms under the plains to about 40 kms under the foothills, and remains constant at this latter value under the Rocky Mountains. Although not a definite conclusion, this interpretation does nonetheless, present an interesting speculation.

Recommendations

We should like to make the following recommendations, since hindsight is better than foresight.

1. More data are required along the Suffield east profile. This line should be extended past Swift Current to obtain first arrival information. Furthermore, the shot holes at Suffield should be drilled into Cretaceous rocks since we have found that shooting in the glacial till results in very poor records.

2. The filter setting should never be lower than 16 cps. Sharp filter bandpass often results in ringing in the filter circuit. Only for very distant shot (over 500 kms) should lower filter settings be used.

3. If at all possible, some sort of communications should be available between the shot point and the recording trucks. Such communication would eliminate much wasted time.

4. A reverse profile should be shot in the mountains to make a definitive interpretation of the crustal structure under the mountains possible. Further work should also be done along the extended line, even if it means using multiple shot holes along this line.

Bibliography

Backus, M. M., Water Reverberations-Their Nature and Elimination, *Geophysics*, *Vol. XXIV*, No. 2, 233-262, 1959.

Blackman, R. B. and J. W. Tukey, The Measurement of Power Spectra, Dover Publications, Inc., New York, 1958.

Bullen, K. E., An Introduction to the Theory of Seismology, Cambridge University Press, 1959.

Cumming, G. L., G. D. Garland and K. Vozoff, Seismological Measurement in Southern Alberta, 1962, Report for ARPA, Project Vela-Uniform.

Dobrin, M. B., Introduction to Geophysical Prospecting, McGraw-Hill Book Co., Inc., 1960.

Eaton, J. P., Crustal Structure from San Francisco, California to Eureka, Nevada, from Seismic-Refraction Measurements, *Jour. of Geophys. Res.*, *68*, no. 20, 5789-5806, 1963.

Ellis, R. M., Analysis of Natural Ultra Low Frequency Electromagnetic Fields, Ph.D. Thesis, University of Alberta, 1964.

Green, R. and J. S. Steinhart, On crustal strusture deduced from seismic time-distance curves, *N. Z. J. Geol. Geophys.*, *5*, 579-591, 1961.

Hall, D. H. and W. C. Brisbin, A Study of the Mohorovičić discontinuity near Flin Flon, Manitoba, Report for ARPA, Project Vela-Uniform.

Healy, J. H., Crustal structure along the coast of California from seismic-refraction measurements, *Jour. of Geophys. Res.*, *68*, no. 20, 5777-5787, 1963.

Hill, D. P., Gravity and crustal structure in the Western Snake River Plain, Idaho, *Jour. of Geophys. Res.*, *68*, no. 20, 5807-5819, 1963.

Hosmer, G. L., Geodesy, John Wiley and Sons, New York, 1929.

Jones, G. H. S., Strong motion seismic effects of the Suffield explosions, Ph.D. Thesis, University of Alberta, 1963.

Jackson, W. H., S. W. Stewart and L. C. Pakiser, Crustal structure in eastern Colorado from seismic-refraction measurements, Jour. of Geophys. Res., 68, no. 20, 5767-5776, 1963.

Kovach, R. L., F. Lehner, and R. Miller, Experimental ground amplitudes from small surface explosions, Geophys., XXVIII, no. 5, 793-798, 1963.

Lee, Y. W., Statistical theory of communication, John Wiley and Sons, Inc., 1960.

McDonal, F. J., F. A. Angola et al, Attenuation of shear and compressional waves in Pierre shales, Geophys., XXIII, no. 3, 421-440, 1958.

McCamy, K., and R. P. Meyer, A correlation method of apparent velocity measurement, Jour. of Geophys. Res., 69, no. 4, 691-700, 1964.

Mota, L., Determination of dips and depths of geologic layers by the seismic-refraction method, Geophys., XIX, 242-254, 1954.

Muskat, M., The theory of refraction shooting, Physics, 4, 14-28, 1933.

Nuttli, O., Seismological evidence pertaining to the structure of the earth's upper mantle, Rev. of Geophys., 1, no. 3, 351-400, 1963.

Pakiser, L. C., Structure of the crust and upper mantle in the western United States, Jour. of Geophys. Res., 68, no. 20, 5747-5756, 1963.

Pakiser, L. C. and D. P . Hill, Crustal structure in Nevada and southern Idaho from nuclear explosions, Jour. of Geophys. Res., 68, no. 20, 5757-5766, 1963.

Richards, T. C. and D. J. Walker, Measurement of the thickness of the earth's crust in the Albertan plains of western Canada, Geophys., XXIV, no. 2, 262-285, 1959.

Richter, C. F., Elementary Seismology, W. H. Freeman and Co., San Francisco, 1958.

Ricker, N., Wavelet functions and their polynomials, Geophys., IX, no. 3, 314-323, 1944.

Ricker, N., The form and laws of propagation of seismic wavelets, Geophys., XVIII, no. 1, 10-41, 1953.

Ricker, N., Wavelet contraction, wavelet expansion and the control of seismic resolution, Geophys., XVIII, no. 4, 769-792, 1953.

Roller, J. C. and J. H. Healy, Seismic-refraction measurement of crustal structure between Santa Monica Bay and Lake Mead, Jour. of Geophys. Res., 68, no. 20, 5837-5849, 1963.

Ryall, A. and D. J. Stuart, Travel times and amplitudes from nuclear explosions, Nevada test site to Ordway, Colorado, Jour. of Geophys. Res., 68, no. 20, 5821-5835, 1963.

Steinhart, J. S. and R. P. Meyer, Explosion studies of continental structure, C.I.W. Publication No. 622, 1961.

Stuart, D. J., J. C. Roller et al, Seismic propagation paths, regional travel times, and crustal structure in the western United States, Geophys., XXIX, no. 2, 178-187, 1964.

Tatel, H. E. and M. A. Tuve, Seismic exploration of a continental crust, Crust of the Earth, G.S.A. Special Paper no. 62, 35-50, 1955.

Veitsman, P. S., The correlation of seismic waves in seismic depth soundings of the earth's crust, Bull. of Acad. of Science of the U.S.S.R., no. 12, 9-28, 1957.

Wadsworth, G. P., E. A. Robinson et al, Detection of reflections on seismic records by linear operators, Geophys., XVIII, no. 3, 539-586, 1953.

Weaver, D., Crustal thickness on Southern Alberta, M.Sc. Thesis, University of Alberta, 1962.

Webb, J. B., Geological history of plains of Western Canada, Western Canada Sedimentary Basin, Rutherford Memorial Volume, AAPG Publication, 3-28, 1954.

Wyrobek, S. M., Application of delay and intercept times in interpretation of multilayer time-distance curves, Geophys. Pros., 4, 112-130, 1956.

Additional Bibliography

Heiskanen, W. A. and F. A. Vening Meinesz, The Earth and its Gravity Field, McGraw-Hill Book Co., Inc.,1958.

Junger, A., Deep Basement Reflections in Big Horn County, Montana, Geophysics, Vol. XVI, 1951.

Garland, G. D., and J. G. Tanner, Investigations of gravity and isostasy in the southern Canadian cordillera, Dom. Obs. Publ., XIX, No. 5, 1957.

Nafe and Drake, Curve of Experimental relationship between compressional wave velocity and density, which was used for gravity calculations. Source of curve is unknown.

Robertson, G., Intrabasement reflections in southwestern Alberta, Supplement to Geophys., XXVIII, No. 5, Pt. II, 1963.

Widess, M. B., and G. L. Taylor, Seismic reflections from Layering within the pre-Cambrian Basement Complex, Oklahoma, Geophys., XXIV, No. 3, 1959.

Appendix 1

Summary of Mathematical Principles Used

There are three sections to this appendix. The first deals with the theory of refraction seismology, for both the case of horizontal layering and that of dipping layers. Reflection seismology is omitted since there were no studies carried out which involved reflected data. Secondly, a statistical section has been developed, showing those techniques used in calculating most of the information presented in this thesis. And finally, since some spectral analyses were carried out, it was felt that there should be at least a cursory glance at the theory of autocorrelation and power spectra derived therefrom.

Where the method of presentation is not my own, I have given credit where credit is due. This is particularly true of the sections dealing with statistics (taken in greater part from Steinhart and Meyer (1961)) and the section on power spectral analysis (taken in greater part from Lee (1960) and from Ellis (1964)).

Mathematical Theory

Section A.

I. Refraction Along N Horizontal Layers.

Case 1. Single Refractor.

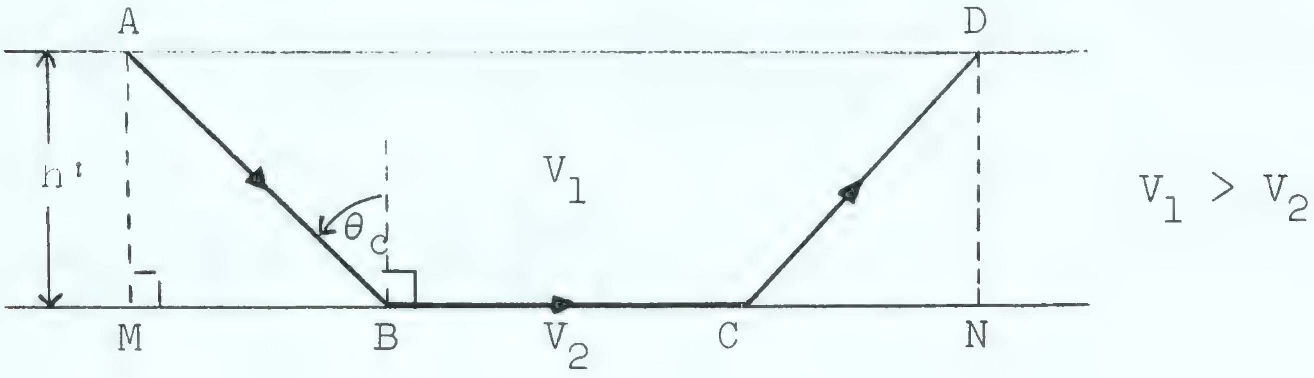

Fig. (A-1)

Consider a ray path as shown in the diagram above. The total time along the path ABCD is given by

$$T = \frac{AB + CD}{V_1} + \frac{BC}{V_2}$$

$$= \frac{AB + CD}{V_1} + \frac{MN}{V_2} - \frac{MB}{V_2} - \frac{CN}{V_2}$$

Now

$$\frac{MB}{h} = \tan \theta_c \qquad \frac{CN}{h} = \tan \theta_c$$

Let $MN = x$

$$\frac{h}{AB} = \frac{h}{CD} = \cos \theta_c$$

and by Snell's Law $\sin \theta_c = \frac{V_1}{V_2}$.

Hence we obtain

$$T = \frac{2h}{V_1 \cos \theta_c} - \frac{2h \tan \theta_c}{V_2} + \frac{x}{V_2}$$

$$= \frac{x}{V_2} + 2h \left[\frac{1}{V_1 \cos \theta_c} - \frac{\sin \theta_c}{\cos \theta_c V_2} \right]$$

$$= \frac{x}{V_2} + \frac{2h}{V_1} \left[\frac{V_2 - V_1 \sin \theta_c}{V_2 \cos \theta_c} \right]$$

$$= \frac{x}{V_2} + \frac{2h}{V_1} \left[\frac{V_2 - \frac{V_1^2}{V_2}}{V_2 \sqrt{1 - (\frac{V_1}{V_2})^2}} \right]$$

$$= \frac{x}{V_2} + \frac{2h}{V_1} \left[\frac{1 - (\frac{V_1}{V_2})^2}{\sqrt{1 - (\frac{V_1}{V_2})^2}} \right]$$

$$= \frac{x}{V_2} + \frac{2h}{V_1} \sqrt{1 - (\frac{V_1}{V_2})^2}$$

$$= \frac{x}{V_2} + \frac{2h \cos \theta_c}{V_1} \qquad (1)$$

The quantity $\frac{2h \cos \theta_c}{V_1}$ is called the intercept time for the first layer. It is the intercept, of the time distance line, at zero distance. This term may be considered as

being composed of two parts, one associated with the shot point, and the other with the detector. It is convenient to call $\frac{h \cos \theta_c}{V_1}$ the delay time; hence the intercept time is the sum of the delay times under the shot and detector.

Case 2. N Refracting Horizons.

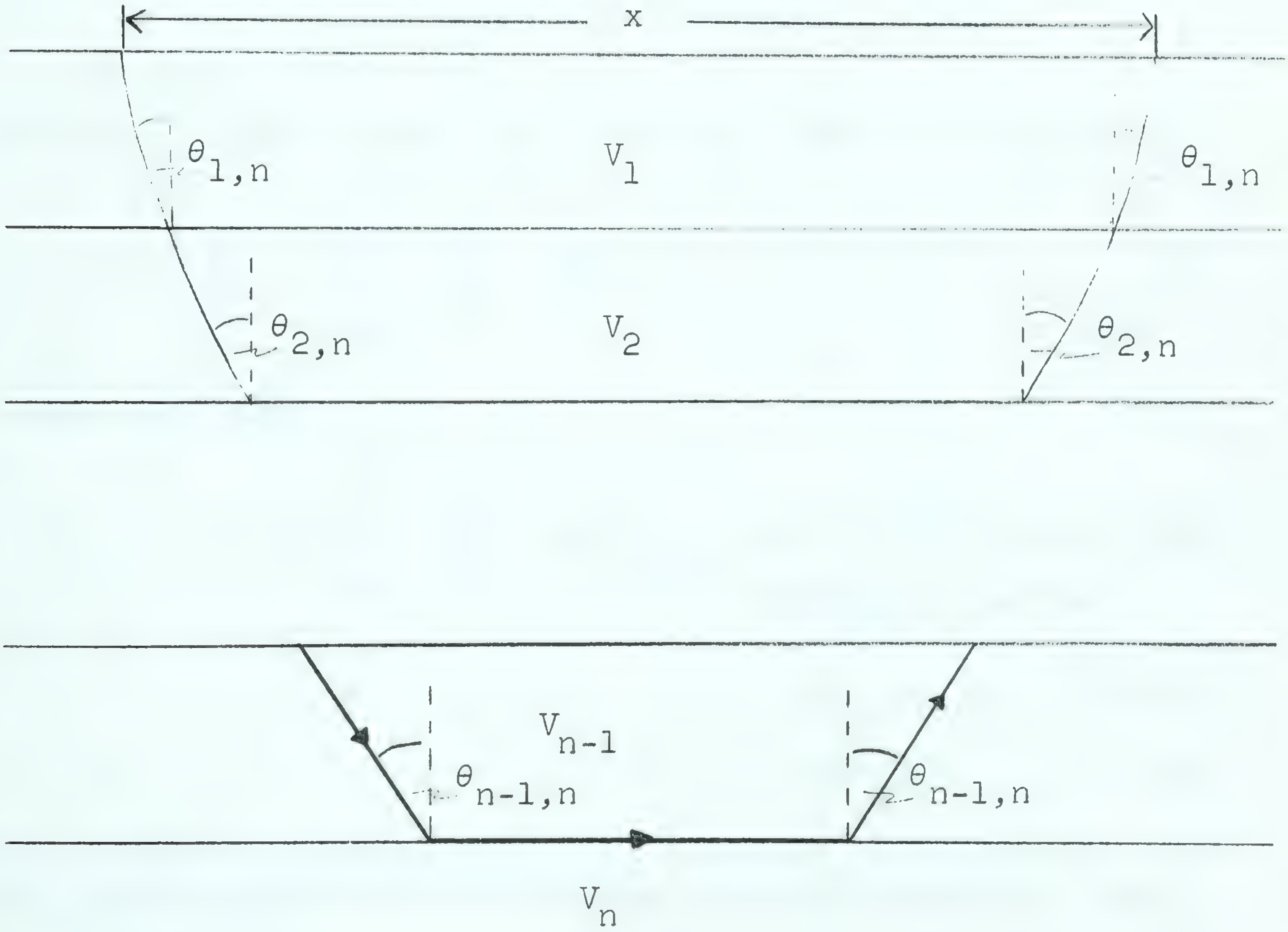

Fig. (A-2)

$$V_1 < V_2 < . \ . \ . < V_{n-1} < V_n$$

The angles $\theta_{1,n}$, $\theta_{2,n}$, . . . $\theta_{n-1,n}$ are defined by Snell's Law as

$$\sin \theta_{1,n} = \frac{V_1}{V_n}$$

$$\sin \theta_{2,n} = \frac{V_2}{V_n}$$

$$\vdots$$

$$\sin \theta_{n-1,n} = \frac{V_{n-1}}{V_n}$$

It can be easily shown that the total time T is given by

$$T = \frac{x}{V_n} + 2 \sum_{i=1}^{n-1} \frac{h_i}{V_i} \cos \theta_{i,n} \qquad (2)$$

where once again

$$2 \sum_{i=1}^{n-1} \frac{h_i}{V_i} \cos \theta_{i,n}$$ = sum of the delay times in the $(n-1)$ layers

= zero distance intercept time (T_n) (3)

If one has refraction data along only one direction, then equation (3) allows one to calculate the various thicknesses h_i of each layer, knowing the various velocities V_i of each layer from the travel-time graph. Furthermore, if one

has data from a double-ended profile, where the intercept times and apparent velocities are such that little dip is indicated in any of the horizons, then equation (3) can again be used to calculate the layer thickness under each shot point. For a double-ended profile where the intercept times and apparent velocities are significantly different, then the equations for dipping layers must be used. A discussion of the dipping layer case follows.

II. Refraction Along N Dipping Layers.

Case 1. Single Refractor.

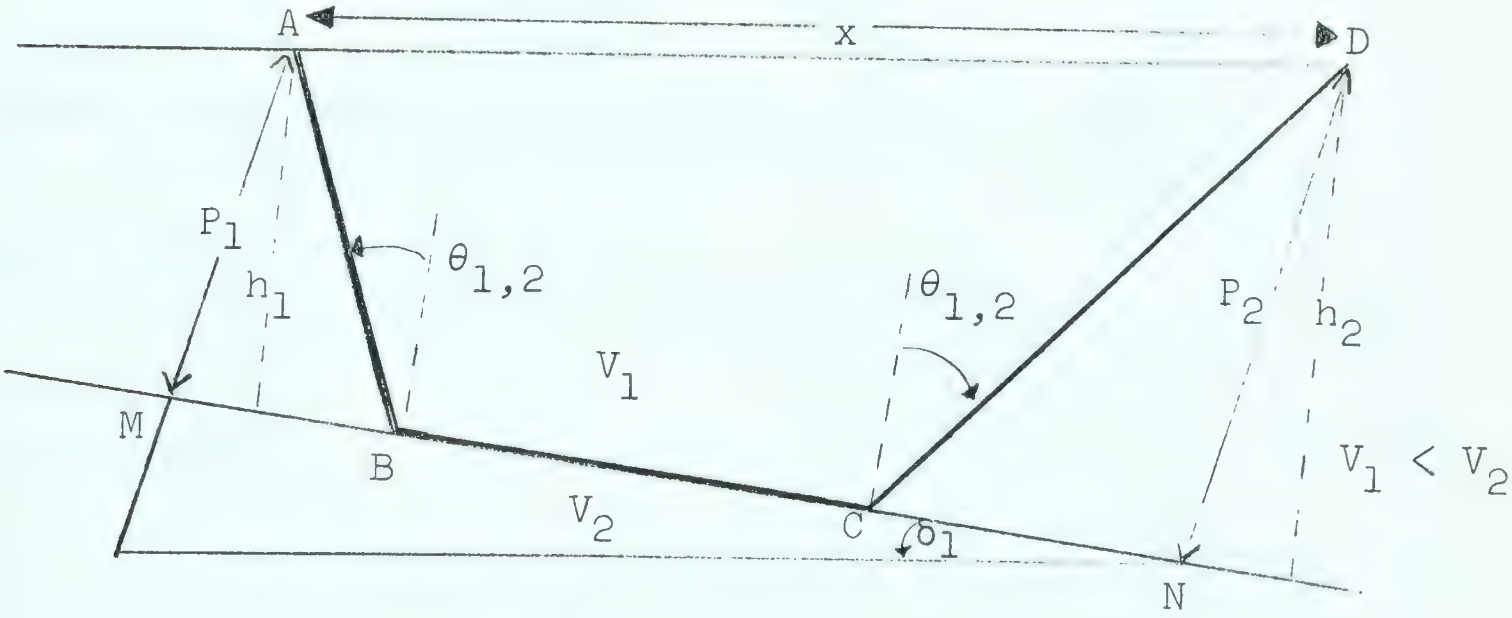

Fig. (A-3)

The total travel time along the ray path ABCD may be written as

$$T = \frac{AB}{V_1} + \frac{BC}{V_2} + \frac{CD}{V_1}$$

$$= \frac{AB}{V_1} + \frac{CD}{V_1} + \frac{MN}{V_2} - \frac{MB}{V_2} - \frac{CN}{V_2}$$

$$= \frac{MN}{V_2} + \left(\frac{AB}{V_1} - \frac{MB}{V_2}\right) + \left(\frac{CD}{V_1} - \frac{CN}{V_2}\right) .$$

We can then make the following substitutions

$$MN = x \cos \delta_1$$

$$MB = P_1 \tan \theta_{1,2} \qquad CN = P_2 \tan \theta_{1,2}$$

$$AB = \frac{P_1}{\cos \theta_{1,2}} \qquad CD = \frac{P_2}{\cos \theta_{1,2}}$$

$$\therefore T = \frac{x \cos \delta_1}{V_2} + \left(\frac{P_1}{\cos \theta_{1,2} V_1} - \frac{P_1 \tan \theta_{1,2}}{V_2}\right) +$$

$$+ \left(\frac{P_2}{\cos \theta_{1,2} V_1} - \frac{P_2 \tan \theta_{1,2}}{V_2}\right)$$

Once again, from Snell's Law we have $\sin \theta_{1,2} = \frac{V_1}{V_2}$

and $T = \frac{x \cos \delta_1}{V_2} + \frac{P_1}{V_1} \cos \theta_{1,2} + \frac{P_2}{V_1} \cos \theta_{1,2}$.

Now we note that

$$P_2 = P_1 + x \sin \delta_1$$

$$\therefore T = \frac{x \cos \delta_1}{V_2} + \frac{2P_1 \cos \theta_{1,2}}{V_1} + \frac{x \sin \delta_1 \cos \theta_{1,2}}{V_1}$$

And using Snell's Law again we obtain finally

$$T = \frac{x}{V_1} \sin \theta_{1,2} \cos \delta_1 + \frac{x}{V_1} \sin \delta_1 \cos \theta_{1,2} + \frac{2P_1 \cos \theta_{1,2}}{V_1}$$

or

$$T = \frac{x}{V_1} \sin (\theta_{1,2} + \delta_1) + \frac{2P_1 \cos \theta_{1,2}}{V_1} \qquad (4)$$

The reciprocal slope, $\frac{V_1}{\sin(\theta_{1,2} + \delta_1)}$, is called the apparent velocity. In order to measure the dip, we must have control along both directions of the profile. If this is indeed the case, then the apparent velocities yield the following information:

$$V_u = \frac{V_1}{\sin (\theta_{1,2} - \delta_1)} = \text{apparent velocity updip} \qquad (5)$$

$$V_d = \frac{V_1}{\sin (\theta_{1,2} + \delta_1)} = \text{apparent velocity downdip} \qquad (6)$$

Hence we obtain

$$\theta_{1,2} = \tfrac{1}{2} \{ \sin^{-1} \frac{V_1}{V_D} + \sin^{-1} \frac{V_1}{V_u} \} = \text{critical angle} \qquad (7)$$

$$\delta_1 = \tfrac{1}{2} \{ \sin^{-1} \frac{V_1}{V_D} - \sin^{-1} \frac{V_1}{V_u} \} = \text{angle of dip} \qquad (8)$$

We can further show that the vertical thicknesses under each end are respectively

$$h_1 = \frac{P_1}{\cos \delta_1} \quad \text{and} \quad h_2 = \frac{P_2}{\cos \delta_1} \qquad (9)$$

The quantity $\frac{2P_1 \cos \theta_{1,2}}{V_1}$ is again the intercept time for the upper layer at point A.

The total travel time equation is often seen in the form

$$T = \frac{R}{V_{an}} + \frac{h_1}{V_1} (\cos \alpha_1 + \cos \beta_1) \qquad (10)$$

where

$R = x$

V_{an} = apparent velocity along the AB direction

$\alpha_1 = \theta_{1,2} - \delta_1$

$\beta_1 = \theta_{1,2} + \delta_1$

This latter form reduces to that form quoted in equation (4)

Case 2. Two Refracting Horizons.

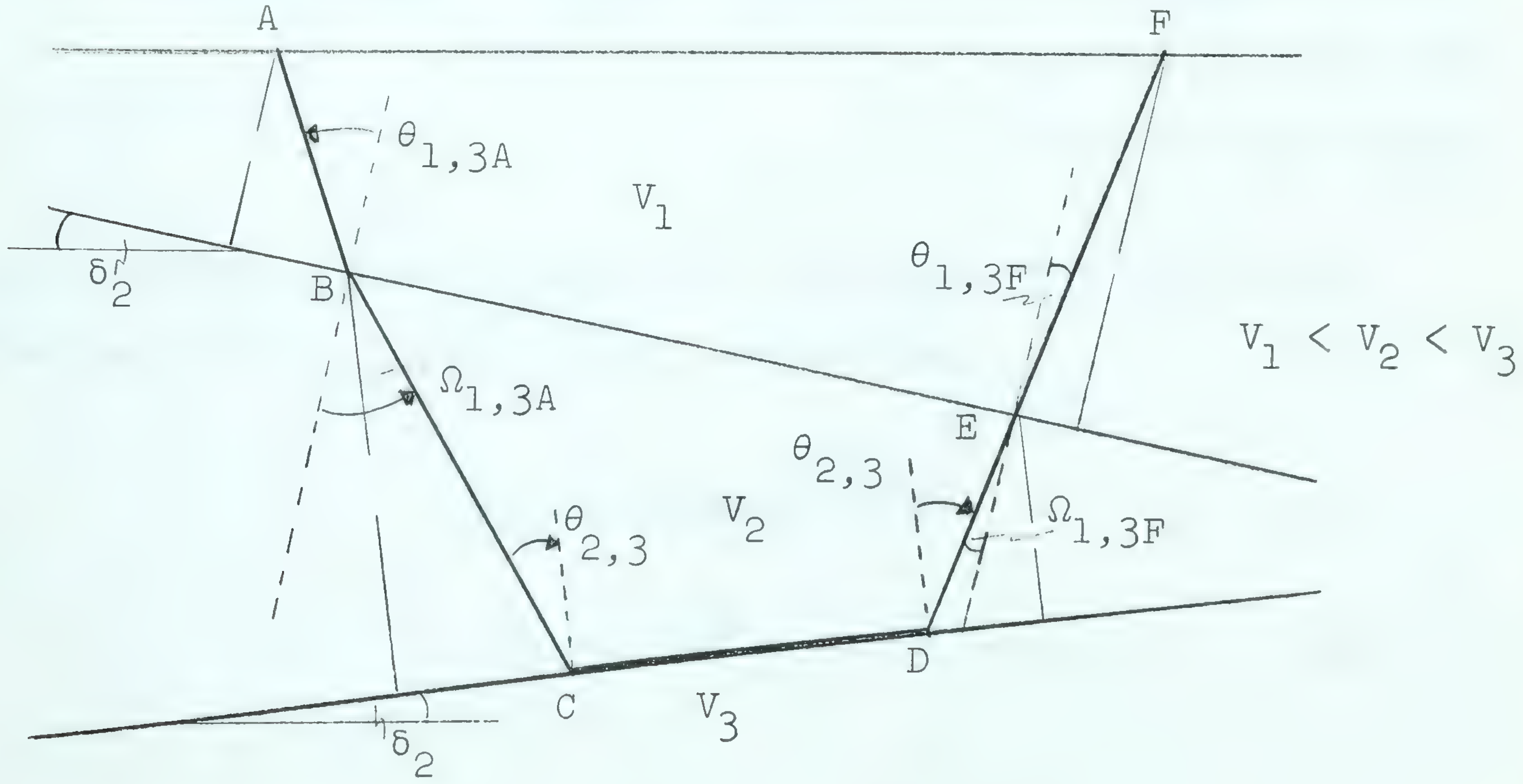

Fig. (A-4)

It is perhaps best to approach this problem from a different point of view. In this case let us think in terms of apparent velocities, V_{A3} being the apparent velocity measured at A, and V_{F3} being the apparent velocity at F, for the 3rd refractor.

$$\left.\begin{aligned} \frac{V_1}{V_{A3}} &= \sin(\theta_{1,3F} + \delta_1) \\ \frac{V_1}{V_{F3}} &= \sin(\theta_{1,3A} - \delta_1) \end{aligned}\right\}$$

These are the angle of emergence relations and may be derived from Snell's Law (11)

From Snell's Law we can obtain directly, the relations

$$\left.\begin{aligned} \Omega_{1,3A} &= \sin^{-1}\left(\frac{V_1}{V_2}\sin\theta_{1,3A}\right) \\ \Omega_{1,3F} &= \sin^{-1}\left(\frac{V_1}{V_2}\sin\theta_{1,3F}\right) \end{aligned}\right\} \quad (12)$$

where $\theta_{1,3A}$ and $\theta_{1,3B}$ are derived from equation (11), and δ_1 is known from previous calculation.

The critical angle $\theta_{2,3}$ and the dip angle δ_2 are simply related to $\Omega_{1,3A}$ and $\Omega_{1,3F}$ as follows:

$$\theta_{2,3} = \frac{\Omega_{1,3A} + \Omega_{1,3F}}{2} \qquad (13)$$

$$\delta_2 = \frac{\Omega_{1,3F} - \Omega_{1,3B}}{2} + \delta_1 \qquad (14)$$

And the true velocity V_3 is given by

$$V_3 = \frac{V_2}{\sin \theta_{2,3}} \tag{15}$$

Solution for the thicknesses under the shot point will be relegated to the N layer case to be discussed next.

Case 3. N Refracting Layers.

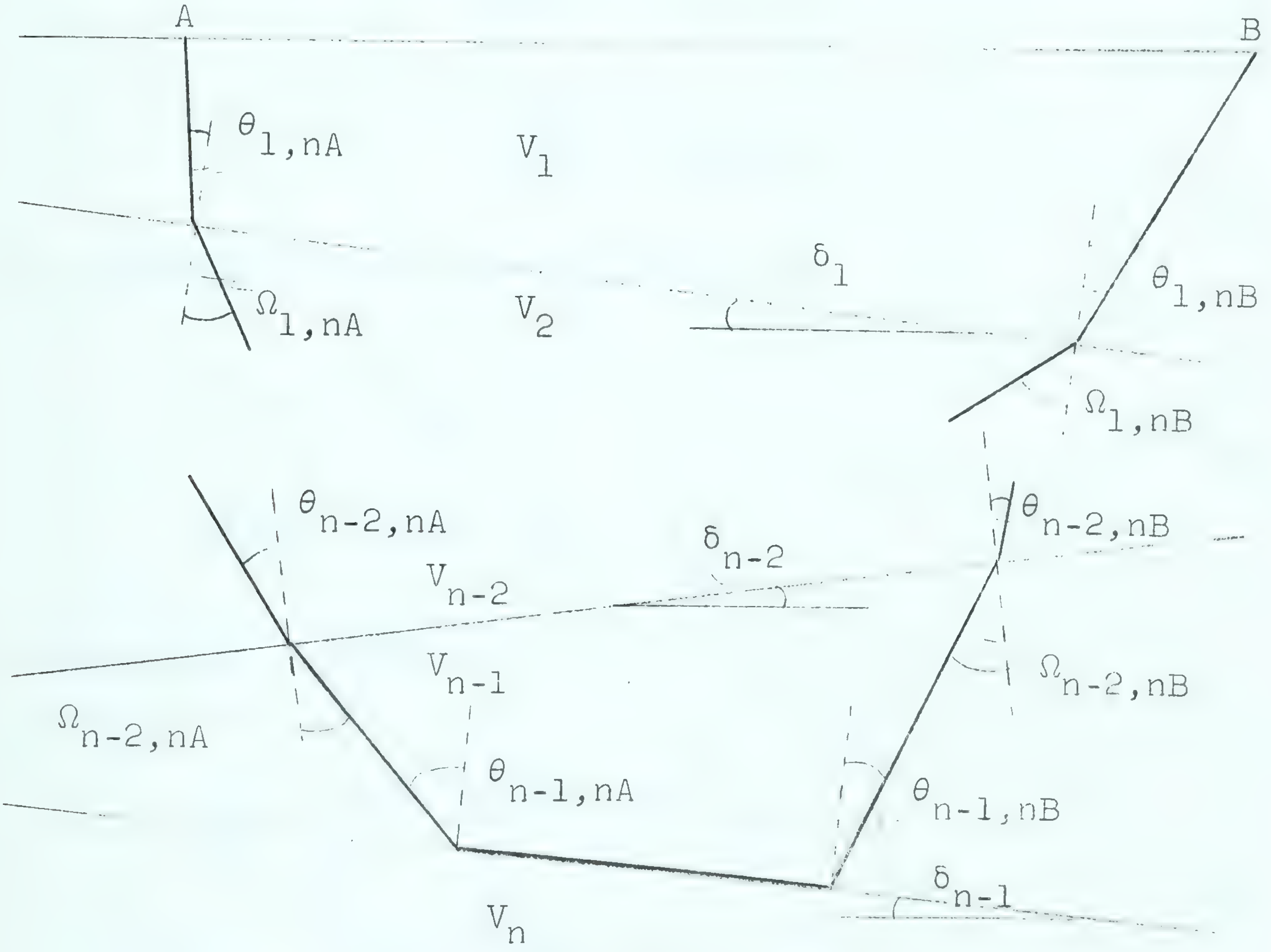

Fig. (A-5)

By analogy to the double refracting case we can write down the following relations:

$$\left.\begin{aligned}\frac{V_1}{V_{nA}} &= \sin\left(\theta_{1,nB} + \delta_1\right)\\ \frac{V_1}{V_{nB}} &= \sin\left(\theta_{1,nA} - \delta_1\right)\end{aligned}\right\} \qquad (16)$$

$$\left.\begin{aligned}\Omega_{1,nA} &= \sin^{-1}\left[\frac{V_2}{V_1}\sin\theta_{1,nn}\right]\\ \Omega_{1,nB} &= \sin^{-1}\left[\frac{V_2}{V_1}\sin\theta_{1,nB}\right]\end{aligned}\right\} \qquad (17)$$

It follows from the geometry then that

$$\left.\begin{aligned}\theta_{2nA} &= \Omega_{1,nA} + \delta_2 - \delta_1\\ \theta_{2nB} &= \Omega_{1,nB} - \delta_2 + \delta_1\end{aligned}\right\} \qquad (18)$$

and then it follows that

$$\left.\begin{aligned}\Omega_{m,nA} &= \sin^{-1}\left[\frac{V_{m+1}}{V_m}\sin i_{m,nA}\right]\\ \Omega_{m,nB} &= \sin^{-1}\left[\frac{V_{m+1}}{V_m}\sin i_{m,nB}\right]\end{aligned}\right\} \qquad (19)$$

furthermore

$$\left.\begin{aligned} \theta_{m,n,A} &= \Omega_{m-1,n,A} + \delta_m - \delta_{m-1} \\ \theta_{m,n,B} &= \Omega_{m-1,n,B} - \delta_m + \delta_{m-1} \end{aligned}\right\} \quad (20)$$

Finally, the critical angle $\theta_{n-1,n}$ is given by

$$\theta_{n-1,n} = \frac{\Omega_{n-2,nB} + \Omega_{n-2,nA}}{2} \quad (21)$$

$$\delta_{n-1} = \frac{\Omega_{n-2,nB} - \Omega_{n-2,nA}}{2} = \text{dip of top of } n^{th} \text{ layer} \quad (22)$$

$$V_n = \frac{V_{n-1}}{\sin \theta_{n-1,n}} = \text{true velocity in } n^{th} \text{ layer} \quad (23)$$

Having obtained these data for each layer, it is then possible to calculate the vertical thickness of each layer under the two shot points. By analogy to the single layer case, we may write the travel time equation as

$$T_A = \frac{R}{V_{an}} + \sum_{i=1}^{n-1} \frac{h_{ai}}{V_i} (\cos \alpha_i + \cos \beta_i) \quad (24)$$

where V_{an} = apparent velocity of n^{th} layer at A

V_i = true velocity of i^{th} layer

$\alpha_i = \theta_{i-1,i} - \delta_i$

$\beta_i = \theta_{i-1,i} + \delta_i$

T_A = travel time along path from A

R = distance from A

h_{ai} = thickness of layer i under A.

Using the zero distance intercept time and reducing equation (24) to a more familiar form we obtain

$$T_{iA} = \sum_{i=1}^{n-1} \frac{2h_{ai}}{V_i} \cos \theta_{i-1,i} \cos \delta_i \qquad (25)$$

The analogous equation at B is written

$$T_{iB} = \sum_{i=1}^{n-1} \frac{2h_{bi}}{V_i} \cos \theta_{i-1,i} \cos \delta_i \qquad (26)$$

Dipping layer theory was used for all the calculations carried out on the data shown in this thesis.

Section B.

Statistical Analyses.

The following discussion is taken from Steinhart and Meyer (1961).

I. Least Squares Line Fitting.

Consider a line whose equation is $T = t_o + \lambda x$ calculated from N points (t_i, x_i). The least squares estimates of the parameters λ and t_o may be found from the following equations

$$\lambda = \frac{\Sigma\, x_i t_i - \dfrac{\Sigma\, x_i\ \Sigma\, t_i}{N}}{\Sigma\, x_i^2 - \dfrac{(\Sigma\, x_i)^2}{N}}$$

$$= \frac{\text{covariance } (x_i, t_i)}{\delta_{xx}} \tag{27}$$

where equation (27) also serves to define δ_{xx}.

$$t_o = \frac{\dfrac{\Sigma\, t_i\, \Sigma\, x_i^2}{N} - \dfrac{\Sigma\, x_i\, \Sigma\, x_i\ t_i}{N}}{\delta_{xx}} \tag{28}$$

This latter equation is somewhat different from that quoted by Steinhart and Meyer (1961) since it was found that this was a more useful form for computational purposes.

Having computed these parameters, it was then possible to calculate the thickness of each of the layers, their dip, and their true velocity using the various equations described in section A.

II. Estimate of the Uncertainty of the Slope λ.

Since the slope is used in the calculations of the crustal model, it seems obvious that we must have some means of describing the uncertainty of the slope. We require the standard deviation (σ_λ) of the slope. Since we have only a finite sample, it is possible to derive only an estimate of σ_λ which we shall call S_λ.

First we must obtain an experimental value for σ_t, the standard deviation of time, and we shall call this S_t. An estimate of σ_t may be obtained from

$$S_t^2 = \frac{\Sigma\,(T - t_i)^2}{N-2} \tag{29}$$

This may be reduced to the following form

$$(N - 2) = S_t^2 = \Sigma\, t_i^2 - \frac{(\Sigma\, t_i)^2}{N} - \frac{\left(\Sigma\, x_i\, t_i - \dfrac{\Sigma\, x_i\, \Sigma\, t_i}{N}\right)^2}{\delta_{xx}} \tag{30}$$

The value of S_t^2 may now be employed to estimate S_λ as follows:

$$S_\lambda^2 = \frac{S_t^2}{\delta_{xx}} \tag{31}$$

The significance of S_λ is not particularly clear as it now stands. A probability statement as regards the limits of uncertainty is perhaps the best way of expressing errors, and this is the type of statement we shall use.

It may be shown rigorously that if ψ is the true value of the slope then λ is distributed normally with mean ψ and variance σ_t^2/δ_{xx}. Since we are dealing with a finite sample, rather than resorting to tables of normal distribution to obtain our probability estimate, we must resort to a table of Student's $\mathcal{T}$ distribution. This is the case since if $\frac{\lambda - \psi}{\sigma_\lambda}$ is normally distributed, then $\frac{\lambda - \psi}{S_\lambda}$ will be distributed according to Student's $\mathcal{T}$ distribution. We can then write the limits of the true value of ψ as follows:

$$\psi = \lambda \pm S_\lambda \mathcal{T}_{N-2} \tag{32}$$

The values used in our calculations were for a probability of 0.1. This implies that nine out of ten time ψ will have a value in the range as calculated using equation (32).

III. Uncertainty of the Time Intercept.

Since we have used the time intercept for calculation of crustal thickness, a statement must be made regarding the uncertainty in t_o. Steinhart and Meyer (1961) use the orthogonal form for the various lines. Thus $T = t_o + \lambda x$ when written in the orthogonal form becomes

$$T = \bar{t} + \lambda\,(X - \bar{x}) \tag{33}$$

where $\bar{t}$ and $\bar{x}$ are the means of t_i and x_i respectively.

Let τ be the true value of T, and using Student's $\mathcal{T}$ we find that

$$\mathcal{T}_{N-2} = \frac{T - \tau}{S_T} \tag{34}$$

where

$$S_T^{\,2} = S_{\bar{t}}^{\,2} + S_\lambda^{\,2}\,(X - \bar{x})^2 \quad \text{and} \quad S_{\bar{t}}^{\,2} = \frac{S_t^{\,2}}{N} \tag{35}$$

If we square $\mathcal{T}_{N-2}$, we can write (34) in the form

$$\mathcal{T}_{N-2}^{\,2} = \frac{d^2}{S_t^{\,2}\left[\frac{1}{N} - \frac{(X - \bar{x})^2}{\delta_{xx}}\right]} \tag{36}$$

where $d = T - \tau$ and $S_\lambda^{\,2} = S_t^{\,2}/\delta_{xx}$.

Equation (36) can be used directly to find the uncertainty in the zero distance intercept time by setting $X = 0$. Thus the confidence limits for τ can be written as

$$(d)_{X=0} = \pm \mathcal{T}_{N-2} \, S_t \left[\frac{1}{N} + \frac{\bar{x}^2}{\delta_{xx}} \right]^{\frac{1}{2}} \tag{37}$$

or

$$\tau = t_o \pm \mathcal{T}_{N-2} \, S_t \left[\frac{1}{N} + \frac{\bar{x}^2}{\delta_{xx}} \right]^{\frac{1}{2}} \tag{38}$$

This completes the discussion of the statistical methods used in analyzing the travel-time graphs and also in postulating our crustal model.

Section C.

The Measurement of Power Spectra.

I. Fourier Analysis.

Let us consider $f(t)$ as being a periodic, piece-wise continuous function, whose integral

$$\int_{-T/2}^{T/2} | f(t) | \, dt < \infty \tag{39}$$

If f(t) satisfies all of these conditions, then it may be expanded in a Fourier Series of the following form

$$f(t) = \frac{a_o}{2} + \sum_{n=1}^{\infty} (a_n \cos nw_1 t + b_n \sin nw_1 t) \qquad (40)$$

where

$$w_1 = \frac{2\pi}{T_1} \quad \text{and} \quad T_1 \text{ is the fundamental period.}$$

We can evaluate the constants a_n and b_n as follows:

$$a_n = \frac{2}{T_1} \int_{-T_1/2}^{T_1/2} f(t) \cos nw_1 t \, dt \quad n = 0, 1, 2, \ldots \qquad (41)$$

$$b_n = \frac{2}{T_1} \int_{-T_1/2}^{T_1/2} f(t) \sin nw_1 \, dt \quad n = 1, 2, 3 \ldots \qquad (42)$$

It is possible to write

$$\cos nw_1 t = \frac{1}{2} (e^{iw_1 nt} + e^{-inw_1 t})$$

$$\sin nw_1 t = -\frac{i}{2} (e^{iw_1 nt} - e^{-iw_1 nt}) \qquad (43)$$

Thus (40) transforms to

$$f(t) = \frac{a_o}{z} + \sum_{n=1}^{\infty} (a_n - ib_n) e^{iw_1 nt} + \sum_{n=1}^{\infty} (a_n + ib_n) e^{-iw_1 nt} \qquad (44)$$

We may further simplify (44) by introducing negative values of n .

$$\left.\begin{aligned} a_{-n} &= \frac{2}{T_1} \int_{-T_1/2}^{T_1/2} f(t) \cos(-w_1 nt)\, dt = a_n \\ b_{-n} &= \frac{2}{T_1} \int_{-T_1/2}^{T_1/2} f(t) \sin(-w_1 nt)\, dt = -b_n \end{aligned}\right\} \quad (45)$$

Therefore

$$\frac{1}{2} \sum_{n=-1}^{-\infty} (a_n - ib_n)\, e^{-iw_1 nt} = \frac{1}{2} \sum_{n=1}^{\infty} (a_n + ib_n)\, e^{iw_1 nt}$$

Thus $f(t)$ may be written in the following form

$$f(t) = \sum_{n=-\infty}^{\infty} F(n)\, e^{iw_1 nt} \quad (46)$$

where $F(n) = \frac{1}{2}(a_n - ib_n)$ $\quad n = 0, 1, 2, \ldots$

and $b_o = 0$.

Combining these various forms we arrive at

$$F(n) = \frac{1}{T_1} \int_{-T_1/2}^{T_1/2} f(t)\, e^{-iw_1 nt}\, dt \quad (47)$$

We note that F(n) is simply the Fourier Transform of f(t). This is a complete function as information regarding amplitude and phase angles is preserved.

F(n) is in general complex, and is called the <u>complex spectrum</u> of f(t). Because the harmonic order n is discrete, the spectrum is called a line spectrum.

In order to demonstrate that indeed amplitudes and phases are preserved, we can write that

$$F(n) = \frac{1}{2}(a_n - ib_n)$$

$$= \frac{1}{2}\sqrt{a_n^2 + b_n^2} \quad e^{i\left[\tan^{-1}\left(\frac{b_n}{a_n}\right)\right]}$$

We define

$$|F(n)| = \frac{1}{2}\sqrt{a_n^2 + b_n^2} \tag{48}$$

as the Amplitude Spectrum of f(t) and

$$\theta_n = \tan^{-1}\frac{b_n}{a_n} \tag{49}$$

as the Phase Spectrum of f(t) .

Therefore we can write

$$f(t) = \sum_{n=-\infty}^{\infty} |F(n)|\, e^{i(w_1 nt + \theta_n)} \tag{50}$$

II. Correlation.

The expression

$$\frac{1}{T_1} \int_{-T_1/2}^{T_1/2} f_1(t)\, f_2\, (t + \tau)\, dt \qquad (51)$$

is of interest, where f_1 and f_2 have the same fundamental angular frequency and τ is a lag time between $(-\infty,\infty)$ and is independent of t. An important property of this function is that its Fourier transform is

$$F_1^*\,(n)\, F_2\,(n) \qquad (52)$$

$F_1^*\,(n)$ being the complex conjugate of $F_1(n)$.

From our previous work we define

$$f_1(t) = \sum_{n\ -\infty}^{\infty} F_1(n) e^{inw_1 t} \qquad f_2(t) = \sum_{n\ -\infty}^{\infty} F_2(n) e^{inw_1 t}$$

$$F_1(n) = \frac{1}{T_1} \int_{-T_1/2}^{T_1/2} f_1(t)\, e^{-iw_1 nt}\, dt$$

$$F_2(n) = \frac{1}{T_1} \int_{-T_1/2}^{T_1/2} f_2(t) e^{-iw_1 nt}\, dt$$

and furthermore

$$f_2(t + \tau) = \sum_{n=-\infty}^{\infty} F_2(n)\, e^{inw_1(t + \tau)}$$

$$\therefore \frac{1}{T_1} \int_{-T_1/2}^{T_1/2} f_1(t)\, f_2(t+\tau) dt = \frac{1}{T_1} \int_{-T_1/2}^{T_1/2} f_1(t) \sum_{n=-\infty}^{\infty} F_2(n) e^{inw_1(t+\tau)} dt$$

$$= \Sigma\, F_2(n) e^{inw_1\tau}\, \frac{1}{T_1} \int_{-T_1/2}^{T_1/2} f_1(t)\, e^{inw_1 t}\, dt$$

$$= \Sigma\, F_2(n)\, F_1^*(n)\, e^{inw_1\tau} \qquad (53)$$

and

$$F_1^*(n)\, F_2(n) = \frac{1}{T_1} \int_{-T_1/2}^{T_1/2} e^{-inw_1\tau} d\tau \int_{-T_1/2}^{T_1/2} f_1(t) f_2(t+\tau)\, dt \qquad (54)$$

We call (54) the Correlation Theorem for periodic functions.

III. Autocorrelation.

The power spectra illustrated and discussed in this thesis were computed using the autocorrelation theorem. Thus for completeness we discuss the autocorrelation function for periodic functions and then simply write the analogous equations for random and quasi-random functions.

If in the correlation theorem $f_1 = f_2$, then

$$\frac{1}{T_1} \int_{-T_1/2}^{T_1/2} f_1(t)\, f_1(t+\tau)\, dt = \sum_{n=-\infty}^{\infty} | F_1(n) |^2 \, e^{iw_1 n\tau} \qquad (55)$$

The left hand side of (55) is called the auto-correlation function and is defined by the symbol $\varphi_{11}(\tau)$. Therefore

$$\varphi_{11}(\tau) = \frac{1}{T_1} \int_{-T_1/2}^{T_1/2} f_1(t)\, f_1(t+\tau)\, dt \qquad (56)$$

Let $\Phi_{11}(n)$ be the Power Spectrum in (55), i.e.,

$$\Phi_{11}(n) = | F_1(n) |^2 \qquad (57)$$

The Autocorrelation Theorem for a periodic function is

$$\left.\begin{aligned} \varphi_{11}(\tau) &= \sum_{n=-\infty}^{\infty} \Phi_{11}(n)\, e^{iw_1 nt} \\ \Phi_{11}(n) &= \frac{1}{T_1} \int_{-T_1/2}^{T_1/2} \varphi_{11}(\tau)\, e^{-iw_1 nt}\, d\tau \end{aligned}\right\} \qquad (58)$$

Furthermore, the autocorrelation function is an even function. That is

$$\varphi_{11}(-\tau) = \frac{1}{T_1} \int_{-T_1/2}^{T_1/2} f_1(t)\, f_1(t-\tau)dt = \frac{1}{T_1} \int_{-\frac{T_1}{2}-\tau}^{\frac{T_1}{2}-\tau} f_1(x) f_1(x+\tau) dx$$

$$= \frac{1}{T_1} \int_{-T_1/2}^{T_1/2} f_1(x)\, f_1(x+\tau)\, dx = \varphi_{11}(\tau) \qquad (59)$$

One can then express equation (58) in terms of cosines.

$$\left.\begin{aligned} \varphi_{11}(\tau) &= \sum_{n=-\infty}^{\infty} \Phi_{11}(n) \cos nw_1\tau \\ \Phi_{11}(n) &= \frac{1}{T_1} \int_{-T_1/2}^{T_1/2} \varphi_{11}(\tau) \cos nw_1\tau\, d\tau \end{aligned}\right\} \qquad (58\text{ a})$$

Let us now extend these equations to cover the random and quasi-random time series.

Weiner Theorem for Autocorrelation.

For the case of the periodic function $f_1(t)$ we recall

$$\varphi_{11}(\tau) = \sum_{n=-\infty}^{\infty} e^{inw_1\tau} \frac{1}{T_1} \int_{-T_1/2}^{T_1/2} \varphi_{11}(\mu) e^{-iw_1 n\mu} d\mu \qquad (56\text{ a})$$

As we allow $T_1 \to \infty$, then we allow $f_1(t)$ to approach the random function. We may show that

$$\lim_{T \to \infty} \frac{1}{T} = \frac{dw}{2\pi} \qquad (60)$$

thus we can write equation (56 a) in the form

$$\varphi_{11}(\tau) = \frac{1}{2\pi} \int_{-\infty}^{\infty} e^{iw\tau} dw \int_{-\infty}^{\infty} \varphi_{11}(\mu) e^{-iw\mu} d\mu \qquad (61)$$

Proceeding parallel to our former discussions of Fourier Transform pairs, we may write

$$\left.\begin{aligned} \varphi_{11}(\tau) &= \int_{-\infty}^{\infty} \Phi_{11}(w)\, e^{iw\tau}\, dw \\ \Phi_{11}(w) &= \frac{1}{2\pi} \int_{-\infty}^{\infty} \varphi_{11}(\tau)\, e^{-iw\tau}\, dw \end{aligned}\right\} \qquad (62)$$

Since $\varphi_{11}(\tau)$ is a real and even function, consequently its transform must be a real, even function; we can thus write the above equations (62) as

$$\left.\begin{aligned}\varphi_{11}(\tau) &= \int_{-\infty}^{\infty} \Phi_{11}(w) \cos w\tau \, dw \\ \Phi_{11}(w) &= \frac{1}{2\pi} \int_{-\infty}^{\infty} \varphi_{11}(\tau) \cos w\tau \, d\tau\end{aligned}\right\} \qquad (62\ a)$$

Thus it appears that $\Phi_{11}(w)$ is the power density spectrum of $f_1(t)$. It may also be shown that it is real, even and non-negative.

IV. Computational Formulae.

Summarized below are the computational formulae used to calculate the autopower spectra. This section is taken from Ellis (1964).

Let $x_1, x_2, \ldots x_n$ represent a time series of data sampled at intervals Δt, and whose mean is zero. (In our case Δt = 10 msecs). The spectrum of this series is only defined to the Nyquist frequency $f_N = \frac{1}{2} \Delta t$, the higher frequencies being aliased into frequencies $f \leqslant f_n$.

The Nyquist frequency of our data is 50 cps. This frequency is sufficiently high such that the problem of aliasing is minimal in our spectra, for the high-cut filter setting of the band pass was never higher than 16 cps and line balancing was always used to minimize any 60 cps components. See fig. (2) for curve of the frequency response of the VLF system for various filter settings.

Let L be a correlation lag index, $L = 0, \pm 1, \pm 2, \ldots \pm (n-1)$ and let J be a frequency index for the $(m + 1)$ equally spaced spectral estimates in the range $0 \leqslant f \leqslant f_N$. The following quantities are computed.

1. Autocorrelation

$$A(L) = \frac{1}{n-L} \sum_{i=1}^{n-L} x_i \, x_{i+L} \quad , \quad A(-L) = A(L) \qquad (63)$$

$$L = 0, 1, 2, \ldots, (n-1)$$

2. Autopower density spectra $\quad J = 0, 1, 2, \ldots, m.$

$$X(J) = \Delta t \sum_{L=-(n-1)}^{(n-1)} D_i(L) \, A(L) \cos\left(\frac{LJ\pi}{m}\right) \qquad (64)$$

where $D_i(L)$ is a weighting function, called the Hanning lag window.

3. The Hanning Window:

We noted in part 2 that the autocorrelation function was modified by a weighting function $D_i(L)$ called a lag window

(Blackman and Tukey, 1958). This has the effect of convolving the Fourier transform of $D_i(\tau)$ [$Q_i(f)$ - the spectral window] with the raw spectra. A simple and widely used lag window (whose use is called "hanning") is given in continuous form by

$$\left.\begin{aligned} D_2(\tau) &= \frac{1}{2}\left(1 + \cos\frac{\pi\tau}{T_m}\right) \qquad & |\tau| < T_m \\ &= 0 & |\tau| > T_m \end{aligned}\right\} \quad (65)$$

where T_m = maximum lag calculated. $D_2(\tau)$ and the corresponding $Q_2(f-f_o)$ are shown in Fig. (A-6). This window concentrates the main lobe of $Q_2(f-f_o)$ near f_o and has rapidly falling sides. In digital calculation $T_m = m\Delta t$.

Hanning lag window

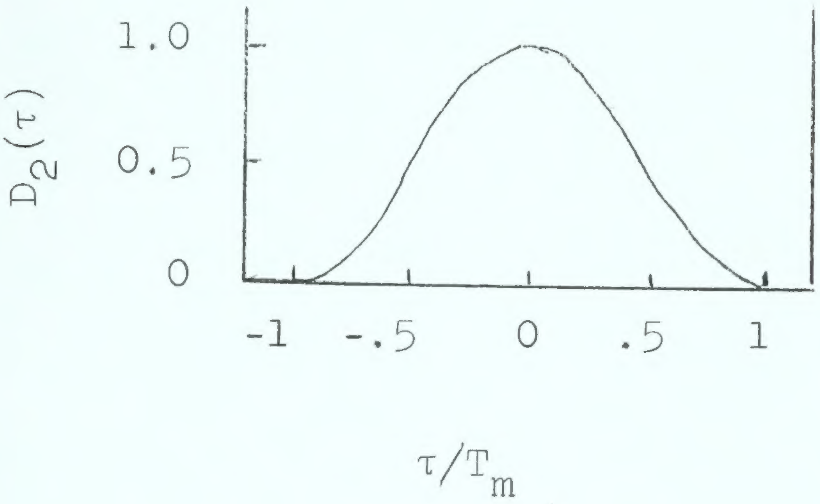

Hanning spectral window

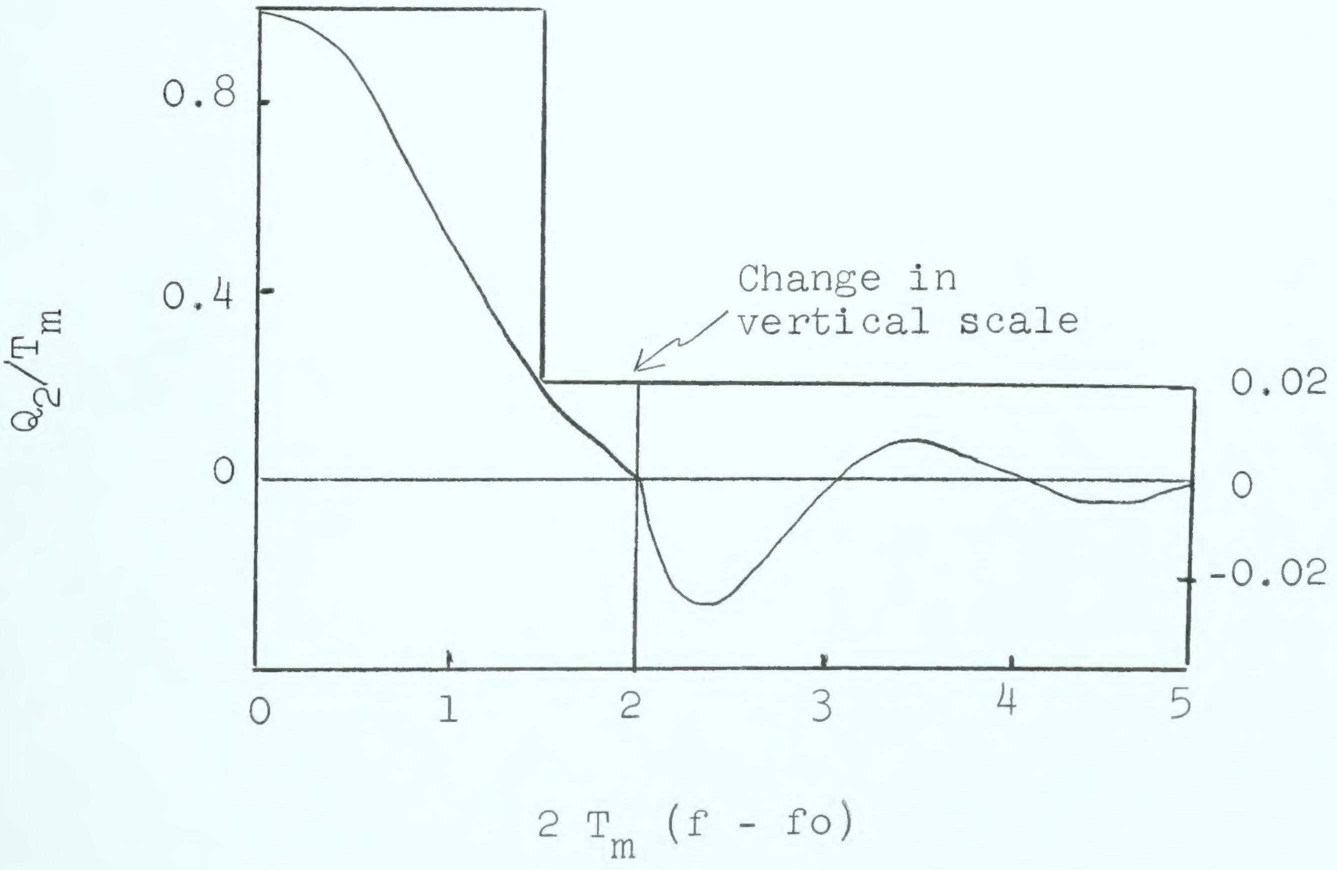

Figure A-6. The lag and spectral window for the hanning estimate (after Blackman and Tukey, 1958).